PROMOTioN
PROGRESS ON MESHED HVDC OFFSHORE TRANSMISSION NETWORKS

WP16 – MMC Test Bench Demonstrator

Deliverable 16.3: Overview of the conducted tests, the results and the associated analyses with respect to the research questions and analyses within WP3

PROMOTioN – Progress on Meshed HVDC Offshore Transmission Networks
Mail info@promotion-offshore.net
Web www.promotion-offshore.net

This result is part of a project that has received funding form the European Union's Horizon 2020 research and innovation programme under grant agreement No 691714.

CONTACT

DOCUMENT INFO SHEET

Document Name:	Deliverable 16.3: Overview of the conducted tests, the results and the associated analyses with respect to the research questions and analyses within WP3
Responsible partner:	RWTH
Work Package:	WP 16
Work Package leader:	RWTH
Task:	Task 16.6: Demonstration of defined test cases regarding interoperability, control schemes and protection
Task lead:	RWTH

DISTRIBUTION LIST

PROMOTioN partners, European Commission

APPROVALS

	Name	Company
Validated by:		
Task leader:	Philipp Ruffing	RWTH
WP Leader:	Philipp Ruffing	RWTH

DOCUMENT HISTORY

Version	Date	Main modification	Author
1.0	27.02.2020		All listed authors

WP Number	WP Title	Person months	Start month	End month
16	MMC Test Bench Demonstrator	106.8	M24	M54

Deliverable Number	Deliverable Title	Type	Dissemination level	Due Date
16.3	Overview of the conducted tests, the results and the associated analyses with respect to the research questions and analyses within WP3	Report	Public	30.01.2020

LIST OF CONTRIBUTORS

Work Package and deliverable involve a large number of partners and contributors. The names of the partners, who contributed to the present deliverable, are presented in the following table.

PARTNER	NAME
RWTH AACHEN	Fisnik Loku, Matthias Quester, Philipp Ruffing,
DNV GL	Yongtao Yang, Andrew Harson, *Andrew Burstein, Yin Sun, Alejandra Fabian (Previously DNVGL)*

EXECUTIVE SUMMARY

Within Work Package 16 of the PROMOTioN project, the operation and control of meshed high-voltage direct current (HVDC) systems as well as their interaction with offshore wind power plants (WPPs) is investigated. While previous work packages of the project, i.e. WP2, WP3 and WP4, focus on simulation-based investigations regarding the challenges associated with the control and protection of future MTDC networks and the connected WPPs, WP16 continuous their analysis using power and control hardware as well as a laboratory scaled MTDC demonstrator.

Within this deliverable, the HVDC converter controls developed in WP2 and the grid forming control of the MMCs developed in WP3 are demonstrated using (lab-scaled) power hardware components. Therefore, a Power-Hardware-in-the-Loop test bench is set up. The obtained laboratory measurements are compared with the corresponding simulation results of a replica model and a full-scale HVDC model. As they are consistent with the simulation results, they help to increase the confidence in the comprehensive simulation studies carried out in WP2 and WP3. While this deliverable focuses on the demonstration of the interoperability between MTDC networks and offshore WPPs during normal operation, the investigations will be extended to dynamic and transient events in the subsequent deliverable D16.4.

The broad stability assessment of converter-dominated networks, like offshore collector networks, requires detailed models of the frequency-dependent impedances of the network's converters. As analytical converter impedance models might not reflect the entire converter behaviour, it is essential to measure their detailed frequency behaviour. Thus, this deliverable presents methods on how to obtain these impedance models from power converters, i.e. wind turbine converters and MMCs, directly from the converter hardware and from their control replicas. The comparison between the impedance measurements obtained from the physical measurements and from their control replicas reveals a close match for frequencies below 1 kHz. The deviations, which can be observed for higher frequencies, are related to limitations of the physical test circuits and the frequency dependent behaviour of power components, which is typically neglected in simulation studies.
In a next step, the obtained frequency-dependent impedances will be used for stability assessments in the frequency domain.

Within WP3 of the project, the black-start capability of wind turbine converters is comprehensibly studied using simulation models. To validate the black-start capability of wind turbines, a commercial wind turbine – again using real hardware and the corresponding replica model – is tested in different start-up modes, i.e. including a soft and a hard start-up. Therefore, suitable testing procedures are developed and demonstrated using real hardware components. These can be used as new tools for manufactures to flexibly and efficiently test converter functionalities and shorten certification processes.
The test results show that the investigated wind turbine converter is able to energise its own offshore AC network and thereby verifies the technology readiness of the black-start functions provided by wind turbine converters.

CONTENT

1 INTRODUCTION

Within the framework of the modernisation of the European electricity grid, multi-terminal HVDC (MTDC) offshore grids evacuating several tens to hundreds of gigawatts of wind power from the Northern Seas shall be integrated into the surrounding AC transmission systems. Additionally, offshore MTDC networks are foreseen as interconnectors between large synchronous zones (e.g. ENTSO-E, UK and the Nordic Grid). Such MTDC systems lead to novel challenges for transmission grid operators, grid planners and manufacturers. However, the experience regarding the operation of these systems as well as their interaction with AC transmission systems and the offshore Wind Power Plants (WPP) is limited.

Within Work Package 16 of the PROMOTioN project, the operation and control of meshed HVDC systems as well as their interaction with offshore WPPs is investigated. While previous work packages of the project, i.e. WP2, WP3 and WP4, focus on simulation-based investigations regarding challenges associated with the control and protection of future MTDC networks and the connected WPPs, WP16 continuous their analysis using power and control hardware as well as a laboratory scaled MTDC demonstrator.

Accordingly, the main objectives of the work package are the:

- **Demonstration** of applicability of developed controls and simulation models of PROMOTioN
- **Technical de-risking** for the deployment and continuous operation of meshed HVDC-systems
- **Improvement** of the feasibility of MTDC grids for road mapping process and standardization efforts

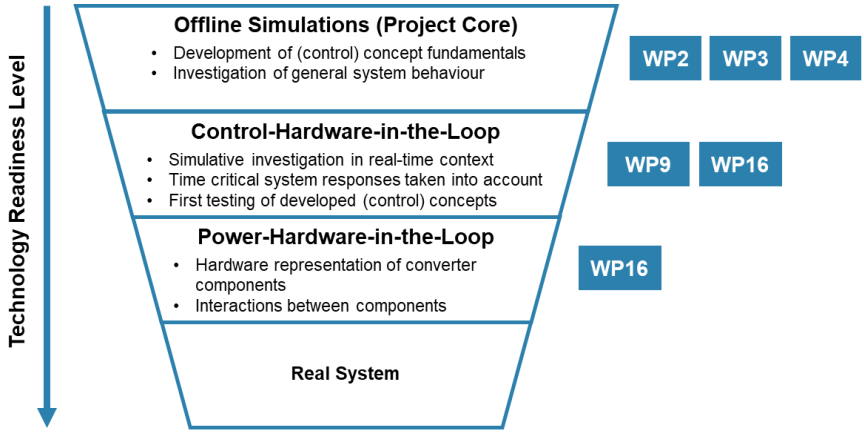

Figure 1-1: Technology-Readiness-Level of converter controls within the PROMOTioN project

This project has received funding from the European Union's Horizon 2020 research and innovation programme under grant agreement No 691714.

1.1 OBJECTIVE AND SCOPE OF WORK

Within this deliverable the common operation of MTDC networks, their HVDC converters and offshore WPPs is studied and demonstrated.

The objectives and main contributions of this work are:

- The interoperability between MTDC networks, their Modular Multi-level Converters (MMCs) and the offshore WPPs has been extensively studied in WP2 and WP3 using electro-magnetic transient simulation (EMT) software tools, i.e. PSCAD|EMTDC™. Control concepts for HVDC networks and the HVDC converters operating in grid forming mode to generator a reference voltage and frequency for the connected WPPs have been studied and enhanced. To validate that these concepts comply with real hardware and independent control units, which e.g. sample on individual internal clocks, a Power-Hardware-in-the-Loop (PHiL) test bench is developed, which connects a physical (laboratory-scaled) HVDC network with a real-time simulation of offshore WPPs. Within this work, the controllability and interoperability of a lab-scale MTDC network connected to offshore WPPs in steady-state conditions is demonstrated. Moreover, the difference between the physical system, its replica model and a full-scaled HVDC model are evaluated.

- Converter dominated power systems and in particular offshore collector networks are associated with a risk of harmonic resonances. To ensure a safe and reliable operation of such networks, it is required to assess their stability over a wide frequency range. Studies investigating harmonic stability are preferably carried out in frequency domain as the required computation time is low and a wide range of scenarios can be investigated [4]. Hence, the frequency responses of the network's converters need to be available as frequency-dependent impedances. Several analytical MMC impedance models have been described in the literature and discussed in PROMOTioN Deliverable D16.5 [1]. However, in real systems the control and the resulting impedance behaviour is typically unknown and might also depend on factors like control modes and operational points. Hence, methods on how to determine the frequency-dependent impedance of voltage source converters (VSCs), i.e. HVDC MMCs and wind turbine (WT) converters, are required. The impedances can be either obtained by measuring the frequency response of the physical converters or their control replicas. In order to formulate best practices on how to determine the frequency-dependent impedance of power converters, test benches for both approaches are established for WT and laboratory-scaled MMC converters as well as for their control replicas. Using these test benches, the power hardware and control replica measurements are compared for MMC and WT converters in order to evaluate both the approaches and give first insights on their applicability.

- Within WP3 of the project, the black-start capability of wind turbine converters is comprehensibly studied using simulation models. To validate the black-start capability of wind turbines, a commercial wind turbine – again using real hardware and the corresponding replica model – is tested in different start-up modes,

This project has received funding from the European Union's Horizon 2020 research and innovation programme under grant agreement No 691714.

i.e. including a soft and a hard start-up. Therefore, suitable testing procedures are developed and demonstrated using lab-scale power hardware.

1.2 OUTLOOK TOWARDS DELIVERBLE D16.4

Since D16.3 is in interim deliverable of WP16, the results and the developed methods directly feed into Deliverable D16.4, which is the final deliverable of the work package. With regard to the common operation of MTDC networks and offshore WPPs, the following points will be included in D16.4:

- While this deliverable focuses on the steady-state operation of a MTDC network connecting offshore WPPs to shore, dynamic and transient situations, like the common fault-ride-through operation in case of faults in the offshore collector grid, will be presented in the upcoming deliverable.
- Based on the obtained frequency-dependent impedance models the stability analysis of offshore HVDC networks will be carried out in frequency domain, i.e. by using the impedance-based stability criterion. The results will then be compared with time-domain simulations and PHiL tests.
- While this deliverable focuses on the demonstration of the black-start capability of a single WT, the black-start tests are extended to the black-start of an entire DRU-connected offshore WPP.

1.3 CONSIDERATIONS FOR THE CONVERTER IMPEDANCE ASSESSMENT

The impedance models are either derived in direct (*d) and quadrature (q) reference*-frame for the WT converter input impedance as well as positive and negative sequence for the MMC input impedance analogous to the analytical impedance models presented in deliverable D16.5 of PROMOTioN [2]. The sequence approach has the advantage that the derived impedances are independent of the grid angle theta at the interconnection point. As a result, the sequence models can also be applied in conjunction with other impedance models not being derived on the basis of a common grid angle. However, deriving models in *dq*-frame is the more intrinsic approach, in particular when controllers are developed in *dq*-frame and the impedance model is analytically derived. In addition, modelling of effects such as cross coupling between frequencies can be implemented easier. To align for future system studies, D16.5 presents transformation matrices to convert models from *dq*-frame to positive and negative sequence. For this, the reader is referred to page 2 and equations (1.1) and (1.2) and section 2.3 of D16.5 [2]. In addition, a discussion of converting impedances between sequence and *dq*-domain and its implications can be found in the literature [3], [4].

This project has received funding from the European Union's Horizon 2020 research and innovation programme under grant agreement No 691714.

2 CONTROL & OPERATION OF WPP CONNECTED TO MESHED HVDC NETWORKS

2.1 INTRODUCTION

One of the main objectives of PROMOTioN WP16 is to demonstrate the network topologies and the controllability of meshed offshore grids developed in PROMOTioN WP2. The differences between the investigations with EMT simulation models and PHiL systems when regarding offshore wind farms (OWFs) connected to a meshed offshore grid have to be investigated so that recommendations for future simulation models can be provided [5]. PHiL investigations with a wind farm emulator and four AC/DC converters connected to a fixed DC bus bar, were carried out in BestPaths project, where the electrical interactions between the DC converter and the wind turbine converters were investigated [6], [7]. In addition to this, the MMC Test Bench comprises of a fully hardware DC grid including four MMC stations. The OWFs and the adjacent AC grids are simulated on real time simulators, which in combination with four linear power amplifiers represent a realistic emulation of the AC grid. The MMC Test Bench in described in detail in deliverable D16.7 “Documentation of the lab set-up, technical specifications and configuration possibilities” [8]. This chapter therefore provides a detailed description of a test case regarding interoperability on MTDC network, its MMCs and offshore WPPs.

Firstly, the system setup used for the investigations in this report is presented and an introduction to the MMC Test Bench as a lab-scaled demonstrator is given. Here, an introduction to the used PHiL interface algorithm to couple the simulated models with the hardware components is introduced.

Secondly, the investigated network including the OWFs and its implementation with the MMC Test Bench is presented in detail. The MMC and the wind turbine control set-up is described as well.

Lastly, the results along with the discussion regarding the controllability of a meshed offshore grid and the interoperability between the MMCs and the WPPs for the simulated test case and the PHiL setup using the MMC Test Bench are presented.

2.2 INVESTIGATED NETWORK AND SYSTEM SET-UP

In this section, the investigated system set-up is described in detail. For the investigations in this report the 4-terminal network configuration developed in the PROMOTioN WP2 with two offshore wind farms (OWFs) and two AC grids is used [5]. The investigated network is shown in Figure 2-1.

This project has received funding from the European Union’s Horizon 2020 research and innovation programme under grant agreement No 691714.

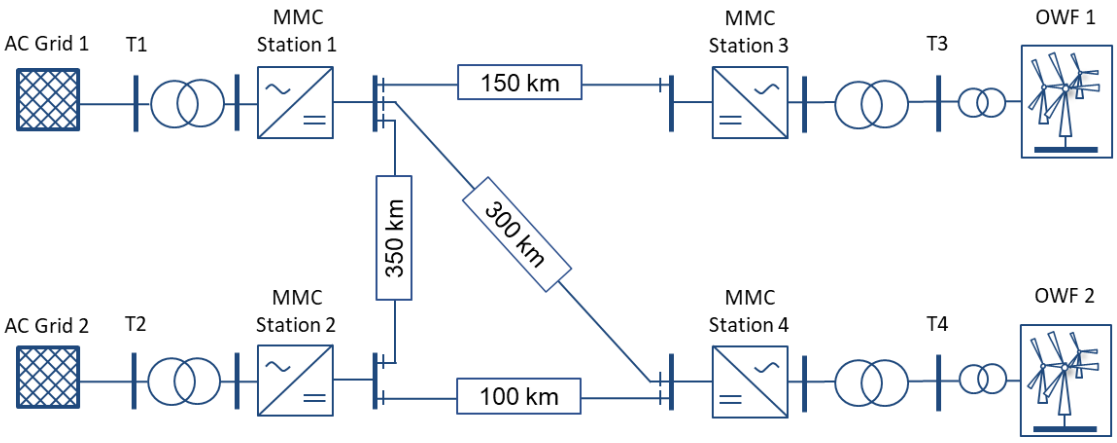

Figure 2-1: The investigated network

Initially, the offline simulated test case model rated as a full-scale model is introduced and then its implementation by using the MMC Test Bench with the corresponding PHiL interface algorithm is explained. The MMC Test Bench implementation is validated against a simulated lab-scale MMC Test Bench digital twin model. Lastly, the system behaviour and the results of the full-scale model, the MMC Test Bench and its lab-scaled digital twin are compared.

2.2.1 OFFLINE SIMULATED FULL-SCALE MODEL

The investigated network consists of MMCs rated at P_{nom} = 1200 MW active power and $V_{DC,n}$ = ± 320 kV DC voltage. The AC grids are simulated as a Thévenin equivalent voltage source with their equivalent grid impedance. The full-scale model is rated at S_{nom} = 30 GVA apparent power and at a rated phase-to-phase AC voltage of $V_{AC,1}$ = 400 kV at f = 50 Hz frequency. The full-scale model parameters of the MMC stations are based on D2.1 [5]. The OWFs are simulated as a synchronous generator and full-scale converter (Type 4) average model, where the IGBT voltage-sourced converters are represented by equivalent voltage sources, which is sufficient for investigations regarding control system dynamics and system interaction [9]. The OWFs are rated at $P_{OWF,nom}$ = 400 MW and consist of 200 2-MW wind turbines connected to a 25-kV distribution system that exports power to a 155-kV grid.

This project has received funding from the European Union's Horizon 2020 research and innovation programme under grant agreement No 691714.

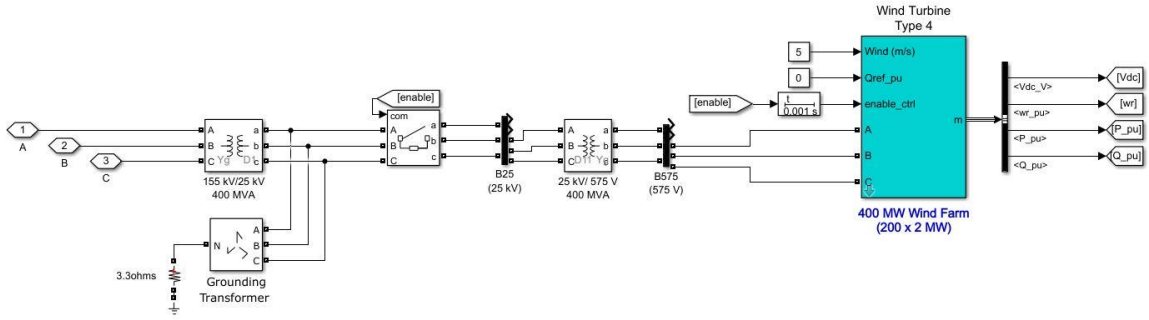

Figure 2-2: Offshore wind farm model

2.2.2 MMC TEST BENCH

The electrical part of the Test Bench system comprises eight monopolar or four bipolar lab-scaled modular multilevel converters (MMC) terminals, DC breaker models and PI sections and four linear power amplifiers (PAs). The schematic system configurations of the monopolar and bipolar MTDC networks are presented in Figure 2-3. Each Test Bench MMC is a three-phase converter comprised of the six arms with a nominal DC voltage of $V_{DC,n}$ = 400 V. The number of cells per arm is 10 and therefore the nominal cell voltage is $V_{c,n}$ = 40 V. The nominal DC current of the MMC is $I_{DC,n}$ = 15 A and the nominal output power of the MMC is $P_{DC,n}$ = 6 kW. Regarding the nominal AC voltage and nominal AC RMS current, the MMC is rated at $V_{AC,1}/V_{AC,2}$= 400/208 V phase to phase and 16.7 A respectively. The switching frequency of the power electronic switches (MOSFETs) can be adjusted as needed for a specific test case. The maximum switching frequency is 10 kHz. The cell capacitors and the arm inductors of the MMC are C_{SM} = 4.92 mF and L_{Arm} = 2.5 mH respectively. The parameters are summarised in Table 2-1 [8].

This project has received funding from the European Union's Horizon 2020 research and innovation programme under grant agreement No 691714.

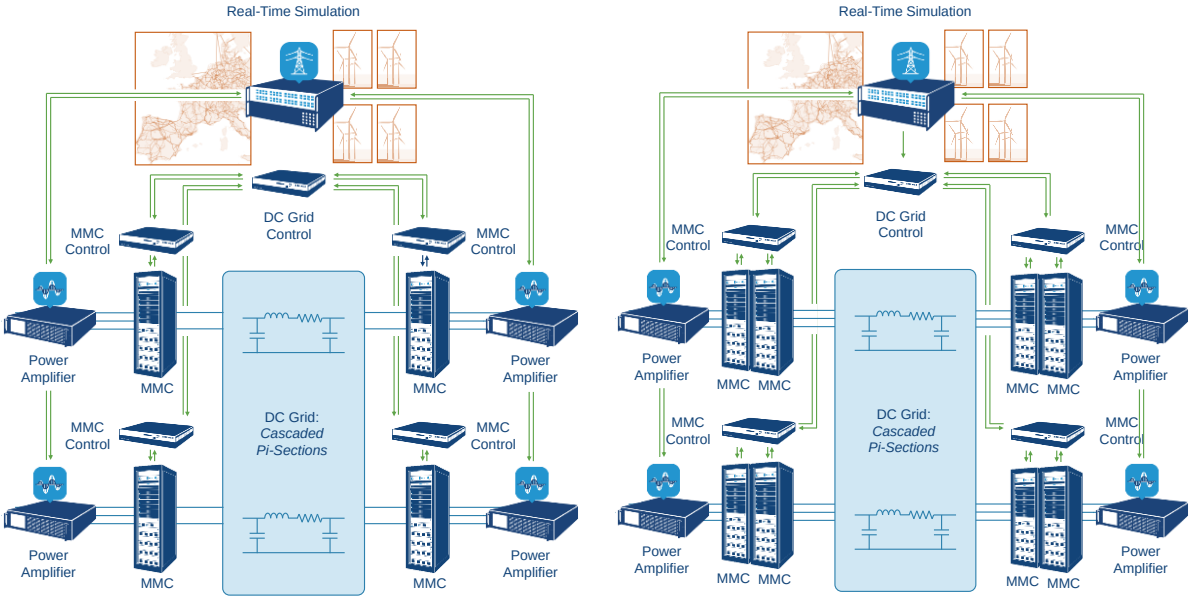

Figure 2-3: Laboratory setup as (a) monopolar and (b) bipolar DC network

Table 2-1: MMC parameters

Nominal DC Voltage	$V_{DC,n}$	400 V
Nominal DC Current	$I_{DC,n}$	15 A
Nominal Output Power	$P_{DC,n}$	6 kW
Nominal AC Voltage per phase	$V_{AC,1}/V_{AC,2}$	400/208 V (3ph-LL)
Nominal AC RMS current at fundamental frequency	I_{AC}	16.7 A
MOSFET Switching Frequency	f_{sw}	0-10 kHz
Number of Cells (Submodules)	n_{SM}	10
Nominal Cell Voltage	$V_{c,n}$	40 V
Cell Capacitor	C_{SM}	4.92 mF
Arm inductor	L_{Arm}	2.5 mH

The submodules can be configured as half-bridge or full-bridge. The submodules are designed for a nominal voltage and current of 40 V and 15 A_{RMS} respectively. The maximum switching frequency of the submodules is 10 kHz and the on/off propagation delay is less than 100 ns. Additionally, the submodule consists of a cell bypass electronic switch, which enables the submodules to be bypassed if required (see Figure 2-4). Furthermore, cell current measurement is also included. The measurements are sent to the controller using a 12-Bit, 500 kbps serial sampling analogue/digital converter (ADC). A fixed hardware instantaneous overcurrent detection is also part of the submodules inner-protection. The galvanic isolation submodule against the control signals is 566 V peak working voltage. The submodule parameters are summarised in

This project has received funding from the European Union's Horizon 2020 research and innovation programme under grant agreement No 691714.

(a)

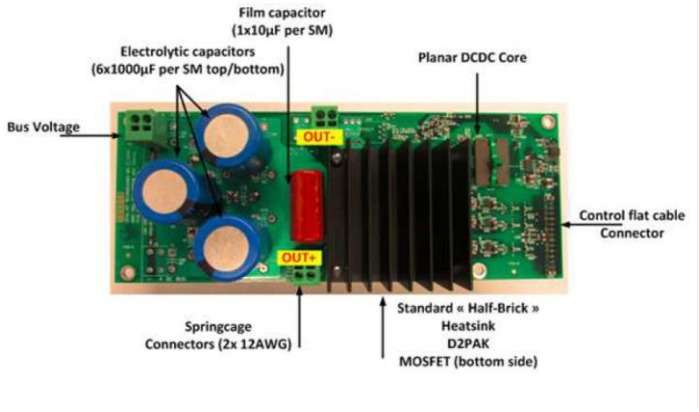

(b)

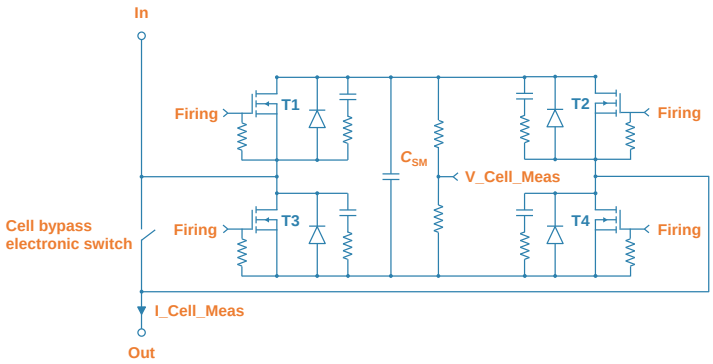

Figure 2-4: (a) picture and (b) equivalent circuit of a submodule [10]

Table 2-2: Submodule Parameters

Submodule designs		half- and full-bridge
Capacitor value	C_{SM}	4.92 mF
Nominal Current	$I_{SM,n}$	15 A_{RMS}
Nominal Voltage	$V_{SM,n}$	40 V
Maximum switching frequency	$f_{SW,Max}$	10 kHz
On/off propagation delay		≤ 100 ns

Table 2-3 shows the transformer parameters that are used in the MMC Test-Bench. Each of the eight 3-phase transformers is integrated in one MMC rack. The transformers are rated at a power of S_{Tr} = 8 kVA and are built in Y/Δ-configuration. The primary side and the secondary side voltages are rated at $V_{Tr,1}$ = 400 V_{RMS} and $V_{Tr,2}$ = 208 V_{RMS} respectively.

This project has received funding from the European Union's Horizon 2020 research and innovation programme under grant agreement No 691714.

Table 2-3: Transformer parameters

Rated Power	S_{Tr}	8 kVA
Configuration		Y/Δ
Nominal primary voltage: Y(phase-phase, RMS)	$V_{Tr,1}$	400 V_{RMS}
Nominal primary voltage: Δ (phase-phase, RMS)	$V_{Tr,2}$	208 V_{RMS}

2.2.2.1 LABORATORY SET-UP

Figure 2-5 shows the schematic laboratory set-up of the investigated test case. The AC grid and the OWF are implemented at full-scale using real time simulators and corresponding simulation tool. The DC grid comprises the lab-scaled MMCs and the Pi-Sections representing the DC cables.

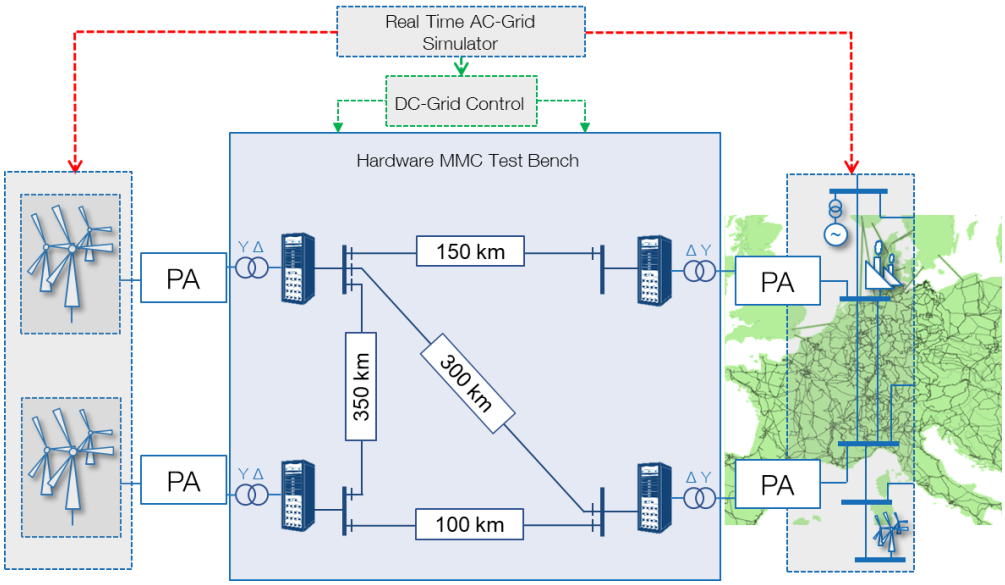

Figure 2-5: Laboratory set-up of the investigated case with Pi-sections as DC cable representation

Cascaded PI sections are used to emulate the cable connections on the DC side of the circuit. The PI sections consist of capacitors and inductors. Separate resistors will not be used since the internal resistance of the inductors is assumed to be close to the line resistance. The parameters of the PI section are provided in Table 2-4. Each PI section represents a length of l_{PI} (± 200 V) = 50 km at a nominal DC voltage of V_{DC} = ± 200 V and l_{PI} (± 400 V) = 25 km at a nominal DC voltage of V_{DC} = ± 400 V. The total number of PI sections is 32.

This project has received funding from the European Union's Horizon 2020 research and innovation programme under grant agreement No 691714.

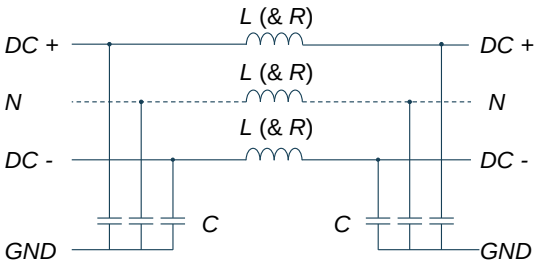

Figure 2-6: DC transmission line model (PI sections)

Table 2-4: Pi Section Parameters

Resistance (inner resistance of the inductor)	R	0.037 Ω
Inductance	L	10 mH
Capacitance	*C*	100 µF

The PI sections are integrated in six PI line cabinets. The connection of the different configuration will be done by using banana cable connections.

2.2.2.2 PHIL INTERFACE

Figure 2-7 shows the PHiL interface algorithm that is used to couple the simulated AC grids and OWF to their respective PAs. Here, the current type ideal transformer method (ITM) is used [11]. The MMC station connected to the OWF is in grid forming control mode and is therefore providing the AC voltage. This voltage is measured, filtered, scaled up and provided as a reference signal to a simulated controlled voltage source (CVS) that is connected to the OWF. The reference voltage signal is scaled according to (2.1):

$$V_{ref} = k_v \cdot \frac{155\ kV}{400\ V} \cdot V_{meas}, \tag{2.1}$$

With:

k_v – being the voltage scaling factor for the analogue communication between the RTS and the PA.

V_{meas} – being the measured voltage at the hardware side of the network.

V_{ref} – being the reference voltage provided to the simulated CVS.

The filter that is used for the measured voltage signals is a lowpass filter with a transfer function according to (2.2):

$$H(s) = \frac{1}{1 + s \cdot T}, \tag{2.2}$$

With:

$T = 1/(2 \cdot \pi \cdot 2000)\ s$ – being the time constant of the lowpass filter.

This project has received funding from the European Union's Horizon 2020 research and innovation programme under grant agreement No 691714.

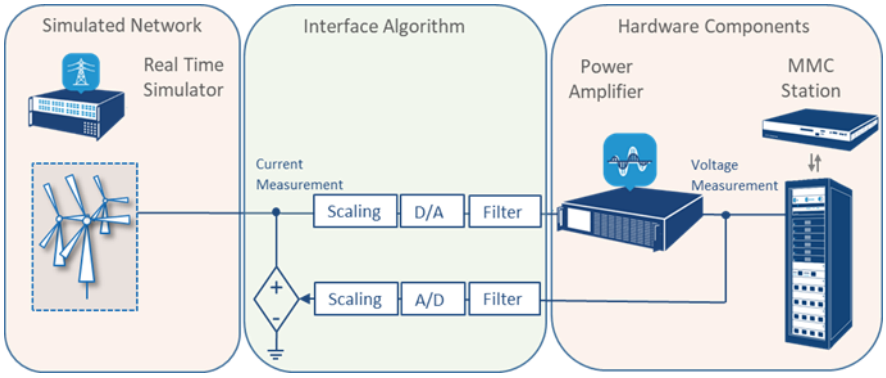

Figure 2-7: PHiL interface algorithm

The current that flows in the simulated circuit is then measured, scaled down and provided to the power amplifier as a reference signal. The reference current signal is scaled according to (2.3):

$$I_{ref} = k_i \cdot \frac{6\ kW}{1200\ MW} \cdot \frac{155\ kV}{400\ V} \cdot I_{meas}, \tag{2.3}$$

With:

k_v – being the current scaling factor for the analogue communication between the RTS and the PA.

I_{ref} – being the reference current provided to the PA.

I_{meas} – being the measured voltage at the software-side of the network.

The power amplifier that receives the reference current signals is in current mode and it provides the corresponding current to the MMC station. On the other side of the circuit, the AC grid is simulated as a stiff grid with the same grid ratings as for the full-scale model. Prior to providing the voltage signals as references to the other power amplifier, they are scaled down to $V_{AC,1}$ = 400 V according to (2.1).

2.2.3 LAB-SCALED MMC TEST BENCH DIGITAL TWIN

The lab-scaled MMC Test Bench digital twin model has the same simulated AC grids and OWFs as the full-scale model. The MMC stations have the same ratings as the MMC Test Bench at P_{nom} = 6 kW active power and a DC voltage of $V_{DC,n}$ = 400 V. Furthermore, additional parasitic resistances of the MMC Test Bench, such as the resistance of the cable connection between the MMC stations and the Pi-sections as well as the connections between the individual PI sections, are integrated in the lab-scaled simulated model. These parasitic resistances are measured for the MMC Test Bench and their impact is discussed in the results.

The connection of the AC grid and the OWF with the lab-scaled DC grid is done by using controlled voltage and current sources, which represent the digital equivalents of the power amplifiers.

PROMOTiON – Progress on Meshed HVDC Offshore Transmission Networks

This project has received funding from the European Union's Horizon 2020 research and innovation programme under grant agreement No 691714.

2.2.4 MMC AND WIND TURBINE CONTROL SET-UP

The control of the MMC is developed in WP2 of PROMOTioN and it is based on Cigre brochure 604 “Guide for the Development of Models for HVDC Converters in a HVDC Grid” [12], [5]. The MMC control is a cascaded vector control and is shown in Figure 2-8. The MMC control is divided into several levels:

- the dispatch controller that provides the controller reference values to the upper level control,
- the upper level control that controls the DC voltage or active power and AC voltage or reactive power to the provided reference values in order to provide the direct (d) and quadrature (q) components of reference current values to the lower level control,
- the lower level control that controls the AC current and provides the reference arm voltage signals,
- the modulation of the reference arm voltages is done in the lower level controls as well.

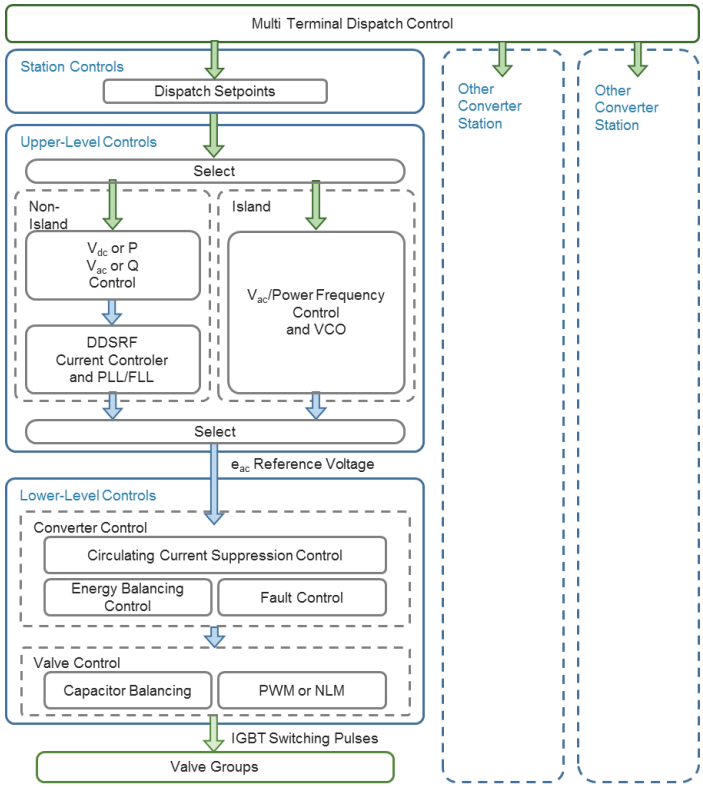

Figure 2-8: Control Hierarchy for MMC-VSC Converters (Based on [12])

The control of the wind turbines is based on [9], [13]. Similar to the MMC control, the WTG control is a cascaded vector control and it is divided into several levels:

- the dispatch controller that provides the DC voltage, reactive power and wind speed reference values,
- the upper level control that controls the DC voltage to provide the d component of the AC current reference, the reactive power and the AC voltage as a cascaded control to provide the q component of the reference current values to the lower level control,
- the lower level control that controls the AC current and provides the reference arm voltage signals.

This project has received funding from the European Union’s Horizon 2020 research and innovation programme under grant agreement No 691714.

- The modulation of the reference arm voltages is done in the lower level controls too.

In addition to the above-mentioned control loops, the WTG control uses the pitch controller to provide the reference pitch angle, which then in combination with the wind speed is used to provide the torque of the wind turbine. The drive train of the wind turbine uses the provided torque by the wind turbine and the generator speed in order to provide the mechanical power for the synchronous machine shaft.

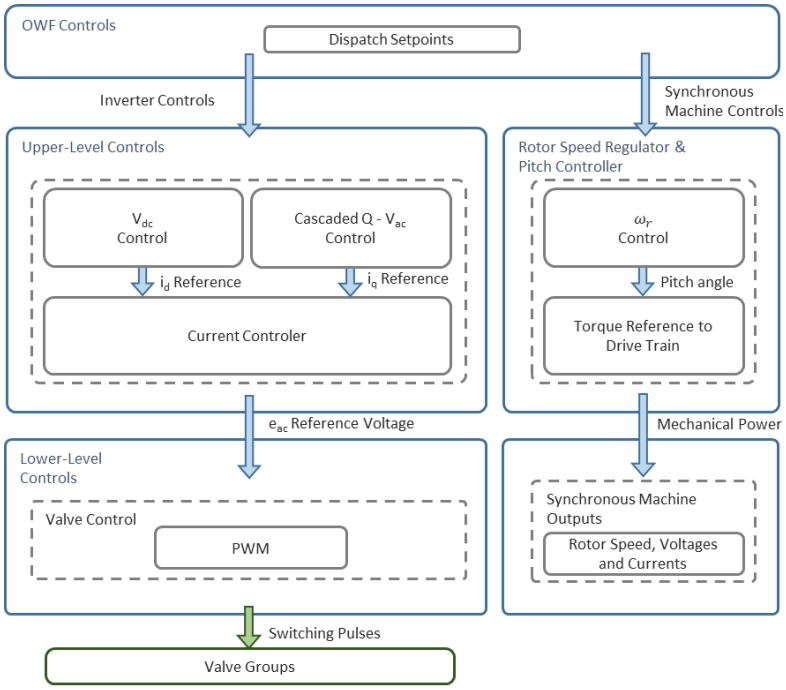

Figure 2-9: Control Hierarchy of the OWFs

2.2.5 TEST CASE OVERVIEW

In the investigated network (see Figure 2-1), MMC station 1 controls the DC voltage and MMC station 2 controls the active power. MMC station 3 and MMC station 4 are operating in grid forming control (GFC) mode and are connected to OWFs. Initially, the network is simulated offline by using MATLAB/SIMULINK©. Then the demonstration of the PHiL set-up of an OWF connection to an MMC station is done. Here, the grid forming control mode of the MMC station is demonstrated and exemplary working points such as the start-up sequence of the OWF and change in wind speed are analysed.

The system is started such that MMC station 1 controls the DC voltage to V_{DC} = 1 p.u. MMC station 2 controls the active power to $P_{C2,ref}$ = -0.3 p.u. Then, MMC station 3 and MMC station 4, which are operating in grid forming control mode, are activated and as soon as the MMC station provides the AC voltage, the respective OWF is connected. The working points of the MMCs are shown in Table 2-5. Different set points regarding the wind speed of the OWF are set, so that a steady state as well as dynamic behaviour can be demonstrated.

This project has received funding from the European Union's Horizon 2020 research and innovation programme under grant agreement No 691714.

Table 2-5 - Converter set points test cases

	MMC STATION 1		MMC STATION 2		MMC STATION 3	MMC STATION 4
Controlling Mode	V_{DC}	Q	P	Q	V_{AC}	V_{AC}
Reference value [p.u.]	1	0	-0.3	0	1	1

2.2.5.1 OFFSHORE WPP START-UP

In this section, the offshore WPP start-up of a single OWF model connected to a MMC station is explained. The other OWF start-up is analogous.

The grid forming control mode of the MMC stations connected to the OWF is activated and the MMC stations are providing a corresponding AC voltage. For the MMC Test Bench, as soon as the MMC grid forming control is activated, the corresponding PA is activated as well, so that the coupling of the simulated OWF and the hardware MMC station is done. The controls of the OWFs are initially disabled. After the desired AC voltage is reached, the AC breaker (see Figure 2-2) is closed and this way connecting the OWF to the MMC station. The OWF controls still remain disabled and initially no current flows from the OWF. 1-2 s after the AC breaker is closed, the controls of OWF are activated and the working point of the OWF is adjusted by controlling the wind speed.

2.2.5.2 CONTROL MODE CHANGES

For the investigated test case, several wind speed fluctuations are investigated in this report. Initially, a steady state with the desired control values shown in Table 2-5 is reached. The wind speed for OWF 2 is defined as constant at v_{wind} = 10 m/s. For OWF 1, the wind speed is changed according to Table 2-6:

Table 2-6 – Wind speed set point changes

2. TEST CASE	OWF 1
Set-point change time	t_3 = at 5 s
From [m/s]	12
To [m/s]	8

The time instances of the set-point changes t_1, t_2, t_3 are defined as the time instance after the steady state of the network is reached.

2.3 RESULTS

The simulated lab-scale model is implemented to represent the digital twin of the MMC Test Bench, rather than the down scaled model of the simulated full-scale model. Therefore, as mentioned in 2.2.3, parasitic resistances such as the resistance of the cable connection from the MMC to the Pi-sections are considered for the lab-scaled model. In order to compare the simulated full-scale model to the simulated lab-scale model and the MMC Test Bench, two cases are considered for the full-scale model:

This project has received funding from the European Union's Horizon 2020 research and innovation programme under grant agreement No 691714.

- The full-scale mode as described in 2.2.1 and developed in D2.1 [5]
- The full-scale model adjusted to represent the full-scale counterpart of the MMC Test Bench: Here, the additional resistances on the DC output of the MMC stations that are measured for the MMC Test Bench are scaled up and included as additional losses on the DC side. The additional resistances are scaled up according to (2.4). The results of this model are noted with the subscript ($_{adj}$).

$$Z_{adj,FS} = Z_{adj,LS} \cdot \frac{(320\ kV)^2}{600\ MW} \cdot \frac{3\ kW}{(200\ V)^2} \tag{2.4}$$

To investigate the behaviour of the system for the simulated models and the MMC Test Bench, the AC voltage, the DC voltage and current as well as the active power is compared for the investigated test case.

Figure 2-10 shows the RMS values of the AC voltages measured at the 4 terminals. At terminal 1 and terminal 2, the AC grids are modelled as strong grids. For the simulated full-scale model and the simulated lab-scale model, the AC voltage has a value of V_{RMS} = 1 p.u. and no difference can be observed. The MMC Test Bench on the other hand shows lower RMS value of the AC voltage. This is due to the reason that the PAs receive the reference voltage values as analogue signals in the range of ± 9 V, and are calibrated to provide the respective line-to-line AC voltage of V_{LL} = ± 400 V. As the same voltage source is implemented in the RTS as for the simulated models, this difference in the RMS AC voltage can be attributed to the calibration of the PA. However, the difference is within the PA calibration error range and is considered as acceptable. This voltage difference can be observed at all 4 terminals. Furthermore, at terminal 3 and 4, the simulated lab-scale model shows higher voltage ripples when compared to the simulated full-scale models. Here, contrary to terminal 1 and 2, where the AC voltage is provided by a strong grid, at terminal 3 and 4, the AC voltage is provided by the MMCs. As the lab-scale MMC model has 10 SM per phase-arm, compared to 350 SM per phase-arm for the full-scale model, it is expected to show higher ripples. The full-scale models show a higher RMS voltage value for 0.002 p.u. Further investigation is needed in this regard. However, for the investigations here, this difference is considered as negligible. The MMC Test Bench shows approximately the same RMS value difference compared to the simulated models as for terminals 1 and 2. Compared to the simulated lab-scale model, the MMCs of the MMC Test Bench have the same number of the SM per phase-arm. However, they are hardware components and are not limited to a simulation time step and therefore show less ripples than their simulated counterpart.

This project has received funding from the European Union's Horizon 2020 research and innovation programme under grant agreement No 691714.

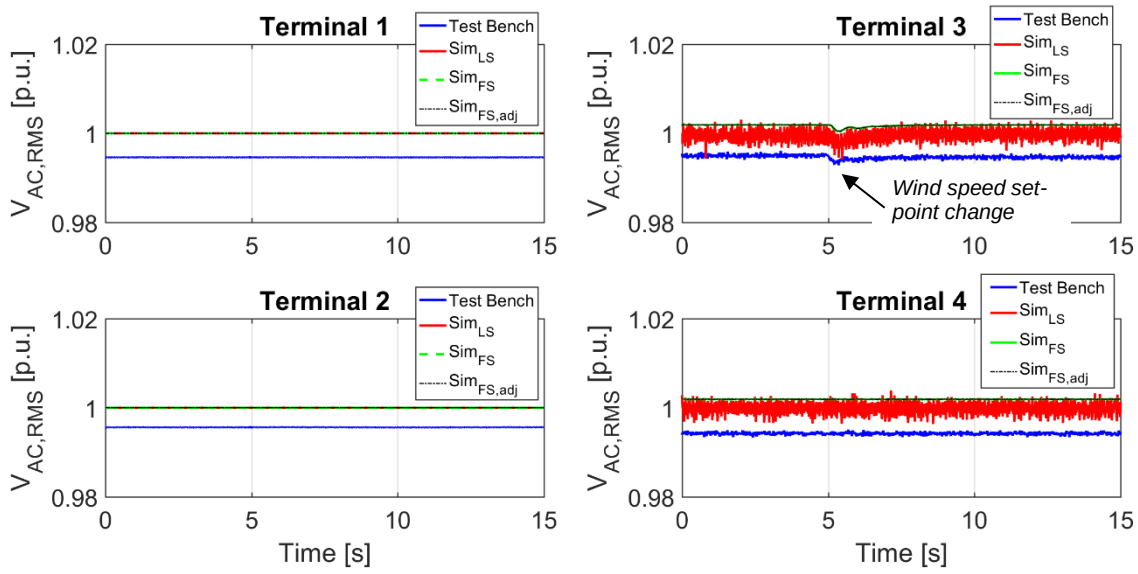

Figure 2-10: AC Voltage RMS value with a wind speed set-point change from v_{wind} = 12 m/s to 8m/s at t = 5 s

Figure 2-11 shows the DC voltage measured at the MMC stations of the investigated network. MMC station 1 controls the DC voltage to V_{DC} = 1 p.u.

If the simulated full-scale mode is considered, where the additional DC line losses ($Sim_{FS,adj}$) are considered, then, apart from the higher ripples of the simulated lab-scale model, the simulated models and the MMC Test Bench show no significant difference. For the simulated full-scale model and the MMC Test Bench, the almost identical DC voltage response to the set-point change of the wind speed at terminal 3 can be observed. At MMC station 2, the simulated lab-scale model and the simulated full-scale model show no difference apart from the higher ripples of the lab-scale model. The DC voltage of the MMC Test Bench at MMC station 2 has a lower amplitude. As MMC station 1 controls the DC voltage and MMC station 2 controls the active power, the lower DC voltage level at MMC station 2 is assumed to be due to the higher transmission line losses of the MMC Test Bench. At MMC station 3 and 4, similar behaviour of the DC voltage as at MMC station 2 can be observed. At MMC station 3, the DC voltage of the simulated lab-scale and full-scale model shows no difference. The DC voltage is initially slightly higher than 1 p.u., since the OWF 1 is at this point exposed to a wind speed of v_{wind} = 12 m/s and consequently it is providing a power of P_{MMC3} = 0.305 p.u. to the DC grid. At t = 5 s, the wind speed set-point is changed to v_{wind} = 8 m/s and the DC voltage at MMC station 3 gets closer to 1 p.u., as the power infeed to the DC grid at this point is lower at P_{MMC3} = 0.12 p.u. The MMC Test Bench shows very similar behaviour to the simulated models. Nevertheless, the difference between the models is considered as minimal and is assumed as acceptable for this report. At MMC station 4, the DC voltage of the simulated models and the MMC Test Bench stays constant, as OWF 2 is exposed to a constant wind of v_{wind} = 10 m/s and therefore provides a constant power to the DC grid. Here, the same differences can be observed as for MMC station 3 for the case when the wind speed for OWF 1 is v_{wind} = 8 m/s.

The original full-scale model (Sim_{FS}) shows no difference to the other models at MMC station 1, as the DC voltage is controlled to V_{DC} = 1 p.u. At MMC station 2 and MMC station 4, where constant power is transferred, the DC

This project has received funding from the European Union's Horizon 2020 research and innovation programme under grant agreement No 691714.

voltage stays at almost the same level after the wind speed at MMC station 3 is decreased at t = 5 s, whereas the other models and the MMC Test Bench experience relatively higher DC voltage decrease. At MMC station 3, Sim_{FS} shows different transient behaviour compared to the adjusted full-scale model ($Sim_{FS,adj}$), the lab-scale model and the MMC Test Bench. Compared to the MMC Test Bench, Sim_{FS} shows for v_{wind} = 12 m/s lower DC voltage level. When the wind speed is changed to v_{wind} = 8 m/s, the DC voltage of the MMC Test Bench drops to a lower level than the DC voltage measured at Sim_{FS}. This difference to the DC voltage behaviour is assumed to be due to the additional losses on the DC grid for the MMC Test Bench, since the lab-scaled model (Sim_{LS}) as well as the full-scale model when the respective DC line losses are considered ($Sim_{FS,adj}$) show a very close behaviour as the MMC Test Bench.

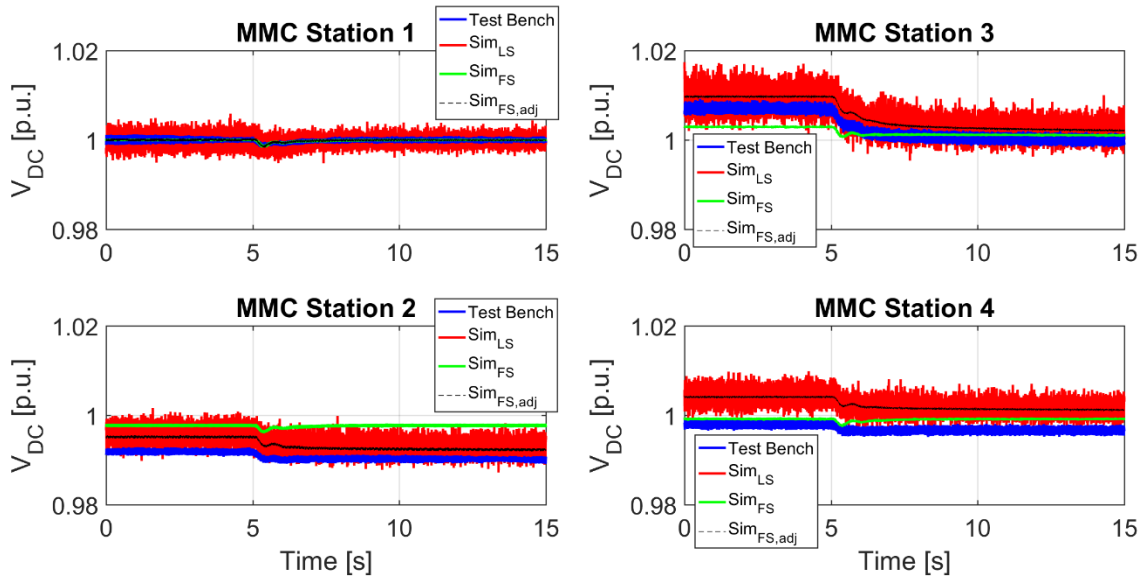

Figure 2-11: DC Voltage

In order to have a closer look at the transient responses between the models, the measured DC voltage at the MMC stations is shown in Figure 2-12 at wind speed set-point change proximity from t = 4.5 s to t = 6.5s. The transient behaviour of the lab-scale model, the full-scale model with the additional DC line losses and the MMC Test Bench can be considered as almost identical.

This project has received funding from the European Union's Horizon 2020 research and innovation programme under grant agreement No 691714.

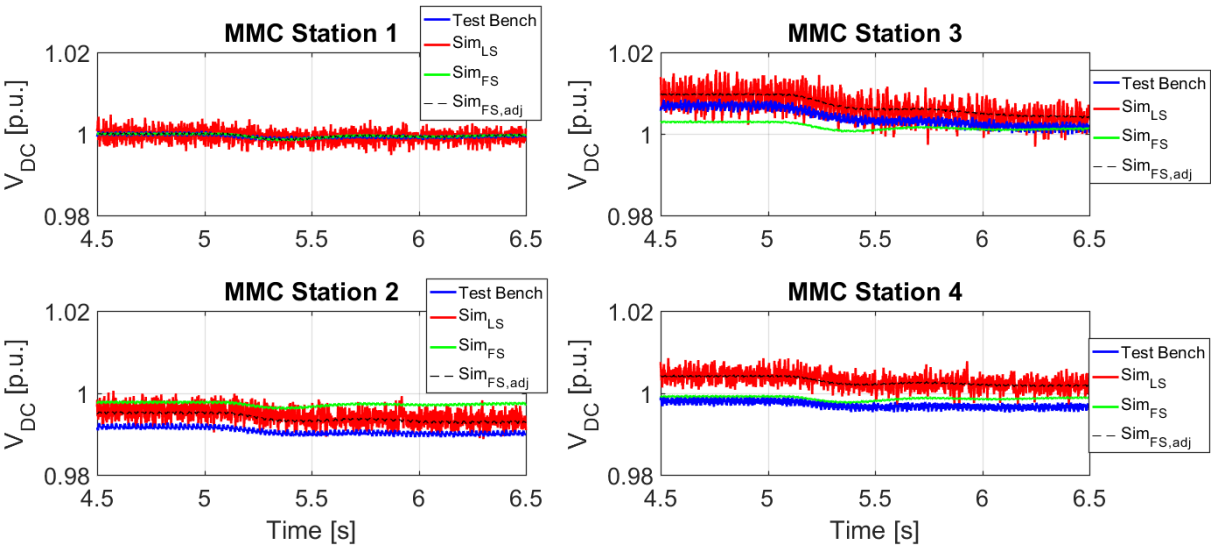

Figure 2-12: DC Voltage

Figure 2-13 shows the DC current measured at the MMC stations. For all the MMC stations, the same behaviour can be observed when the simulated lab-scale and full-scale models as well as the MMC Test Bench are compared against each other. The simulated lab-scale and the full-scale models show no difference except for the higher ripples of the simulated lab-scale model, which are present due to the different number of SM of the corresponding MMC. MMC station 2 and MMC station 4 have constant DC currents, as MMC station 2 controls the active power to P_{MMC2} = 0.3 p.u and absorbs a constant DC current of $I_{DC,MMC4}$ = -0.32 p.u. MMC station 4 is exposed to a constant wind speed and accordingly provides a constant DC current of $I_{DC,MMC4}$ = 0.18 p.u. MMC station 3 is initially providing a current of $I_{DC,MMC3}$ = 0.3 p.u. to the DC grid and after t = 5 s, a DC current of $I_{DC,MMC3}$ = 0.109 p.u. The DC current at MMC station 1 is just the difference between the DC currents provided by the MMC station 3 and 4 and the DC current absorbed at MMC station 2. The MMC Test Bench shows the same behaviour of the DC current as for the simulated models, with the only difference being the lower magnitude of the DC current. This is assumed to be due to the calibration error of the PA 3 and PA 4, which are in current mode and provide the current measured at the simulated OWF 1 and OWF 2, respectively. The calibration factor of the current mode of the PAs is also assumed to be within its limits and is not further investigated in this report. At MMC station 1 the DC current of the MMC Test Bench shows lower amplitude relative to the simulated models when compared to the other MMC stations. This is due to the reason that at MMC station 3 and MMC station 4 for the MMC Test Bench, where the DC current is fed into the DC grid, is already lower than the simulated model and at MMC station on this difference is added. Otherwise, at MMC station 1, the DC current shows the same transient behaviour for the set-point change as for instance the simulated full-scale model.

This project has received funding from the European Union's Horizon 2020 research and innovation programme under grant agreement No 691714.

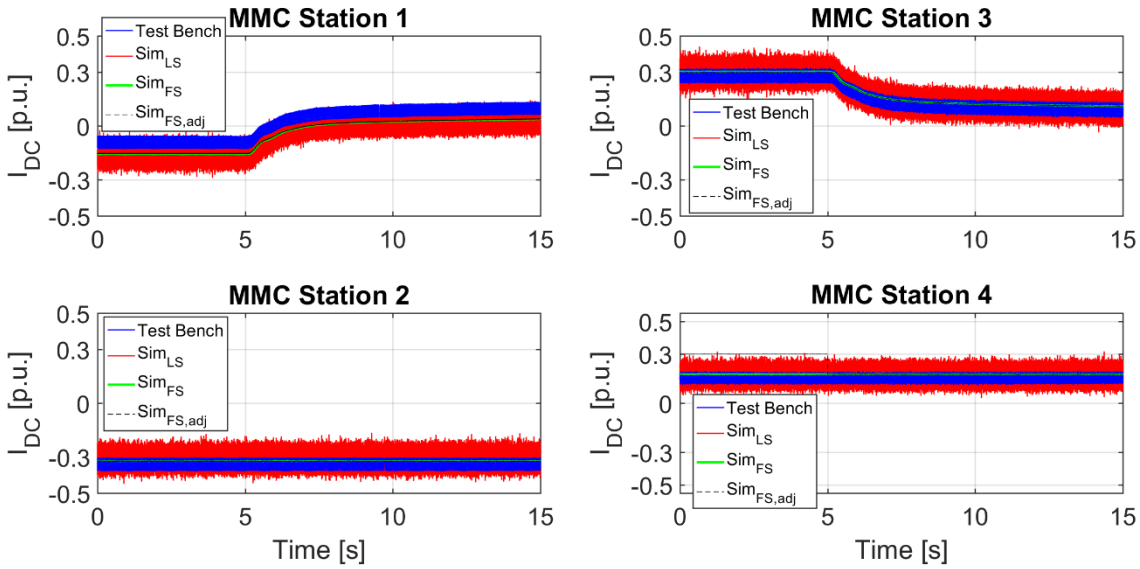

Figure 2-13: DC Current

Figure 2-14 shows the active power measured at the terminals. The active power plots show very similar behaviour when compared to the DC current plots. At terminal 2, the active power is controlled to a constant value of P_{MMC2} = 0.3 p.u. The simulated models and the MMC Test Bench show no significant difference. The ripples of the simulated lab-scale model and the MMC Test Bench arise due to their number of SM per phase-arm. At terminal 3, OWF 1 is initially exposed to a wind speed of v_{wind} = 12 m/s and it provides an active power of P_{MMC3} = 0.3 p.u. For this wind speed set-point, the simulated models and the MMC Test Bench show very close behaviour. Apart from the ripples, there is no other significant difference between the simulated models and the MMC Test Bench. At t = 5 s, the wind speed set-point is changed to v_{wind} = 8 m/s. During the transient period of the wind speed change, the active power of the simulated models and the MMC Test Bench shows no significant difference and after the steady-state of this wind speed set-point, OWF 1 provides an active power of P_{MMC3} = 0.116 p.u. to the DC grid. At terminal 4, the simulated models and the MMC Test Bench show no difference too. Here, OWF 2 is exposed to a constant wind speed of v_{wind} = 8 m/s, and therefore the simulated models and the MMC Test Bench provide an active power of P_{MMC3} = 0.179 p.u. At terminal 1, initially the difference between the generated active power from OWF 1 and OWF and the absorbed active power by AC grid 2, is absorbed. At t = 5 s, as the active power provided by the OWF 1 decreases, terminal 1 provides active power to the DC grid, such that the active power at terminal 2 stays constant at P_{MMC3} = -0.3 p.u. At terminal 1, the simulated models show no difference apart from the ripples. The active power of the MMC Test Bench has for the first wind speed set-point lower magnitude when compared to the simulated models. As already described in this report, this difference is assumed to be due to the higher DC line losses for the MMC Test Bench. The same can be observed if the second wind speed set-point is observed. Here, MMC station 1 at terminal 1 has to provide an active power terminal 2, so that it can compensate the reduced power infeed from OWF 1. However, since the distance from terminal 1 to terminal 2 is 350 km, compared to the distance from terminal 3 to terminal 1 of 150 km when terminal 1 was absorbing the excess power infeed from the OWFS, the DC line losses for the second

This project has received funding from the European Union's Horizon 2020 research and innovation programme under grant agreement No 691714.

wind speed set-point will be higher. This can be seen at terminal 1, where the difference between the MMC Test Bench and the simulated models is larger than the difference between the MMC Test Bench and the simulated models for the initial wind speed set-point.

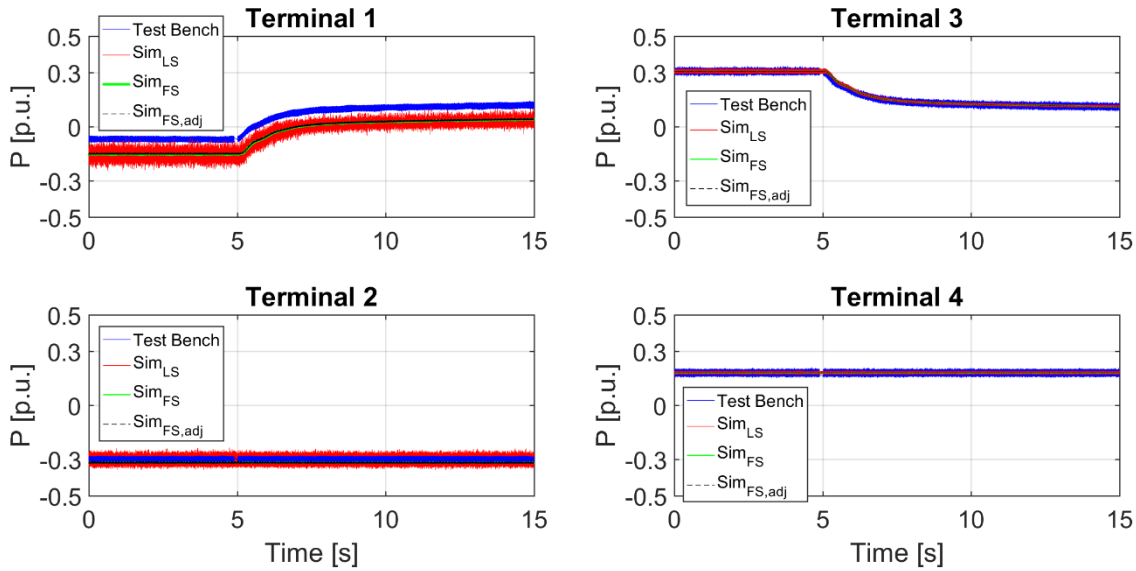

Figure 2-14: Active power

2.4 DISCUSSION

In this report, the 4-terminal network configuration developed in the PROMOTioN WP2 with two OWFs and two AC grids [5] is considered. Initially, the 4-terminal network is scaled down and is implemented using the MMC Test Bench. Different wind speed set-points are implemented and the resulting AC voltage, DC voltage and current and the active power transfer at the 4 terminals is analysed and the simulated models are compared to the MMC Test Bench. Furthermore, the MMC controls developed in WP2 and the grid forming control of the MMCs developed in WP3 are demonstrated using the MMC Test Bench. Overall, the results show a very close match between the simulated lab-scale model and the MMC Test Bench. Regarding the full-scale model, when additional resistances are considered, that represent full-scaled counterpart of the cable losses from the MMC stations to the PI-sections in the MMC Test Bench, then the system behaviour of the simulated models and the MMC Test Bench shows no significant difference. In this case, the main difference between the simulated full-scale model and the simulated lab-scale model is the fact that the simulated lab-scale model shows higher ripples for the AC voltage provided by the grid forming MMC stations, the DC voltage and current and the active power. However, this is expected as the number of the SM per phase-arm between the models differ. The lab-scale MMC model has 10 SM per-phase arm, whereas the full-scale MMC model has 350 SM per-phase arm and if the simulation time step of Δt_{sim} = 40 µs is considered, then the quality of the generated voltage and current signals will be affected. As modulation technique for the full-scale mode, the nearest level modulation (NLM) is used. For the lab-scale model, a combination of the NLM and the pulse-width modulation (PWM) is used, such that the NLM determines the minimal number of the inserted SMs and the PWM determines whether an additional SM is

This project has received funding from the European Union's Horizon 2020 research and innovation programme under grant agreement No 691714.

inserted or not. The MMC Test Bench on the other hand has the same number of SM per phase-arm as the simulated lab-scale model, but the MMCs allow the switching of the SMs every 500 ns. Therefore, the MMC Test Bench shows lower ripples then the simulated lab-scale model. The modulation technique used for the MMC Test Bench is the same as for the lab-scale model. Furthermore, the results in this report show that the DC line losses for the MMC Test Bench are higher than in the simulated models. When the original full-scale model, i.e. without the additional DC line losses is considered, there is a difference in the transient behaviour of the full-scale model compared to the lab-scale model and the MMC Test Bench. Further investigations regarding the reduction or elimination of the additional parasitic losses in the MMC Test Bench will be carried out. One possible solution could be to substitute the existing connections between the MMCs and the Pi-section with cables with a larger diameter, to reduce the parasitic resistance of the connection between the MMC stations and the Pi-sections. Furthermore, the additional DC line losses that come from the cable connections between the Pi-sections will be investigated as well and corresponding measured will be considered, such that the MMC Test Bench shows a closer behaviour to the original full-scale model, which serves as a reference. Overall, this investigation demonstrates the developed controls in WP2 and WP3 in PROMOTioN using the 4-terminal network developed in PROMOTioN [5], Hereby, it is demonstrated that the MMC Test Bench and the developed control algorithms can be used for further investigations, such as the interactions between HVDC converters and active AC-networks, e.g. OWFs, black start capability of OWFs connected via HVDC, validation of developed frequency-dependent MMC impedance models.

Moreover, it is shown that the developed controls comply with the real hardware and the independently controlled converters and WPPs. Thereby, the results can raise the confidence in the deliverable control algorithms.

This project has received funding from the European Union's Horizon 2020 research and innovation programme under grant agreement No 691714.

3 WIND TURBINE INPUT ADMITTANCE MEASUREMENT AND VALIDATION

3.1 OVERVIEW

Modern power systems comprising a high level of voltage source converters (VSCs) are associated with a risk of harmonic resonances, which is one of the major objectives of the PROMOTioN WP16. The theoretical framework of the harmonic resonance analysis (i.e. impedance-based analysis) was summarized for two-level and Modular Multi-Level VSC in Deliverable 16.5, respectively [1]. This chapter summarises the lab setup and results concerning the frequency dependent input-impedance measurement of an MW-scale wind turbine generator (WTG) converter and its control replica demonstrator realized in DNV GL Flex Power Grid Lab, Arnhem, the Netherlands. The specific objectives are:

- Propose a power test circuit (henceforth referred as PHiL) for the measurement of the input-impedance of a vendor specific wind turbine power converter unit (i.e. a commercial 1-MW WTG power converter unit, henceforth referred as Device-Under-Test (DUT))
- Establish a Controller-Hardware-in-the-Loop (CHiL) setup to measure the input-impedance of the wind turbine controller replica of the same vendor
- Compare the input-impedance measurement results in the PHiL setup with its counterparts in the CHiL setup and provide recommended practices for the future industrial application.

3.2 WTG INPUT IMPEDANCE TEST SETUP

For the physical PHiL setup, a MW-level AC-side input-impedance[1] measurement test bench is established as shown in Figure 3-1.

A 1.32 MW DC supply operates as a current source feeding the DC-link of the DUT directly. The amplifier is externally controlled by a real-time simulator (RTS) to inject a perturbation current at the point of connection (PoC), where the WTG typically connects the 690 V side of its step-up transformer (see red measurement point of i_{abc} and V_{abc} in Figure 3-1. Passive circuits (including transformer, cables and current/voltage sensors) are also shown in Figure 3-1. Due to the unavailability of a grid emulator in the lab, the grid-connected WTG converter is connected to the 10.5 kV medium voltage (MV) grid via three step-up transformers (i.e. autotrafo, TR6 and TR2). In addition, a current perturbation circuitry is established for the MW-level input-impedance measurement. Compared to the voltage perturbation method, the current perturbation method has several advantages:

- The kW-level input-impedance setup typically employs a linear or a high bandwidth switching voltage source, the voltage perturbation signal can be directly superimposed on the fundamental frequency component. Since a voltage perturbation source would need to sink all the fundamental frequency current

[1] This is the AC side harmonic impedance as measured at the point of connection towards the wind turbine. It is called “input impedance“, since it measures the opposition of the WTG to current into its internal circuit. The source impedance of the external grid is called “output impedance” in that context. https://en.wikipedia.org/wiki/Input_impedance

This project has received funding from the European Union’s Horizon 2020 research and innovation programme under grant agreement No 691714.

produced by the DUT (i.e. the perturbation source has to match the rating of the DUT), a current perturbation source is preferable for the MW-scale test circuit.

- The power converter output bandwidth (the frequency bandwidth of the generated voltages and currents from the power converter) is generally inversely proportional to its rating. For the voltage perturbation source matching the rating of the DUT in the MW-level, it is difficult to produce a high bandwidth voltage source that can excite the circuit in a wide frequency range unless a high order multi-level topology is used.
- The perturbation current i_{perb} is a series of sinusoidal waveforms with varying frequencies in order to measure the input impedance of the DUT for the whole bandwidth. It is programmed within and generated by the Power Amplifiers (Egeston[2]).

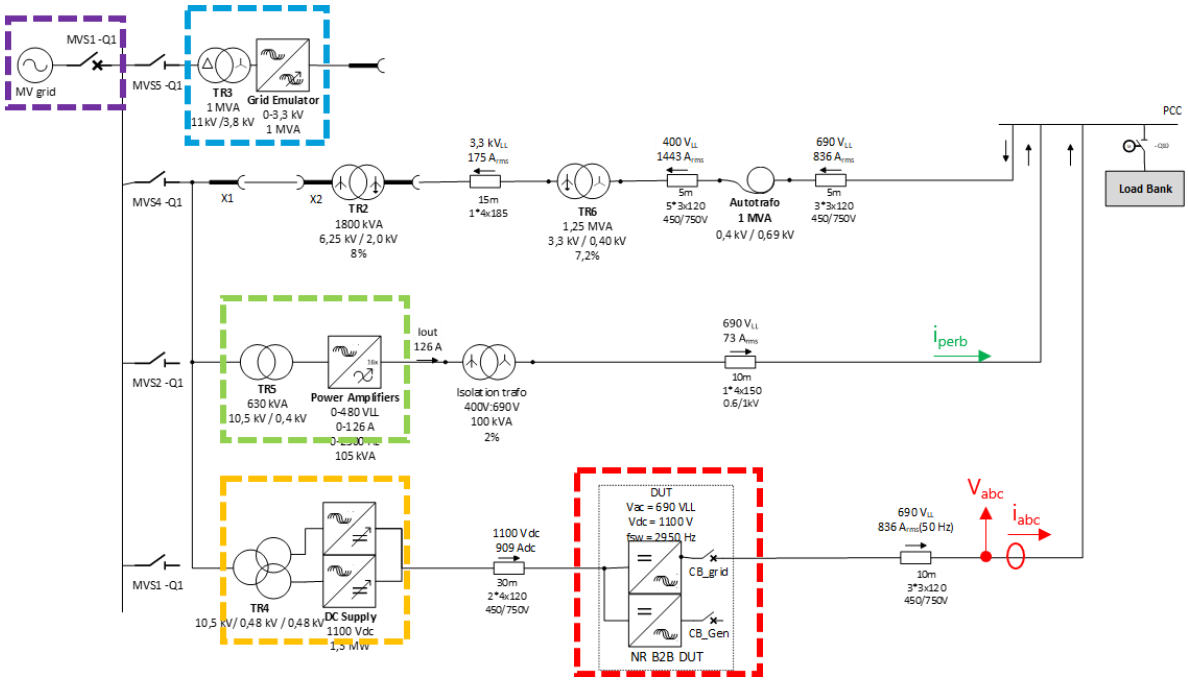

Figure 3-1: PHiL setup for the WTG power converter input-impedance measurement

Similarly, a CHiL is established to work with a controller replica of the WTG power converter from the same vendor, with the current perturbation method applied. In Figure 3-2, the grid side current/voltage signals (i.e. $I_{\mathrm{g,abc}}$ and $V_{\mathrm{g,abc}}$) and generator side current/voltage signals (i.e. $I_{\mathrm{gen,abc}}$ and $V_{\mathrm{gen,abc}}$) are calculated in the RTS[3] and exported via its analogue output interface. The analogue output signal from the RTS will then interface with the WTG controller replica by providing 10 V signals. The controller replica calculates the IGBT switching pulses for both the generator-side converter as well as the grid-side converter. The RTS will interface with the IGBT switching pulses from the controller replica utilising its time-stamped digital input interface. The generator breaker, the grid breaker, and the soft-charging breaker in the RTS model are interfaced with the controller replica via the static digital input (e.g. close and open command) and output (e.g. returning the breaker position).

[2] EGSTON: www.egstonpower.com

[3] OPAL-RT: www.opal-rt.com

This project has received funding from the European Union's Horizon 2020 research and innovation programme under grant agreement No 691714.

The PSCAD simulation were carried out by the vendor using its in-house WTG model with the identical parameters as the DUTs in the PHiL and the CHiL setup.

Both PHiL and CHiL setup are established to measure the input-impedance of the 1-MW WTG power converter. On the one hand, the aim is to verify the feasibility of the current perturbation method in the PHiL setup as it allows the input-impedance measurement of a DUT, i.e. the 1-MW WTG converter, which has a higher power rating than the perturbation source itself. On the other hand, the aim is to establish the benchmark for the PHiL input-impedance measurement and compare it with the CHiL results. Thereby, the measurements obtained in the CHiL approach are verified against the PHIL measurements. The results from the offline PSCAD simulation are also provided here to illustrate the potential impact of Hardware-in-the-loop test as compared with pure off-line digital simulation. The current perturbation method is also applied here.

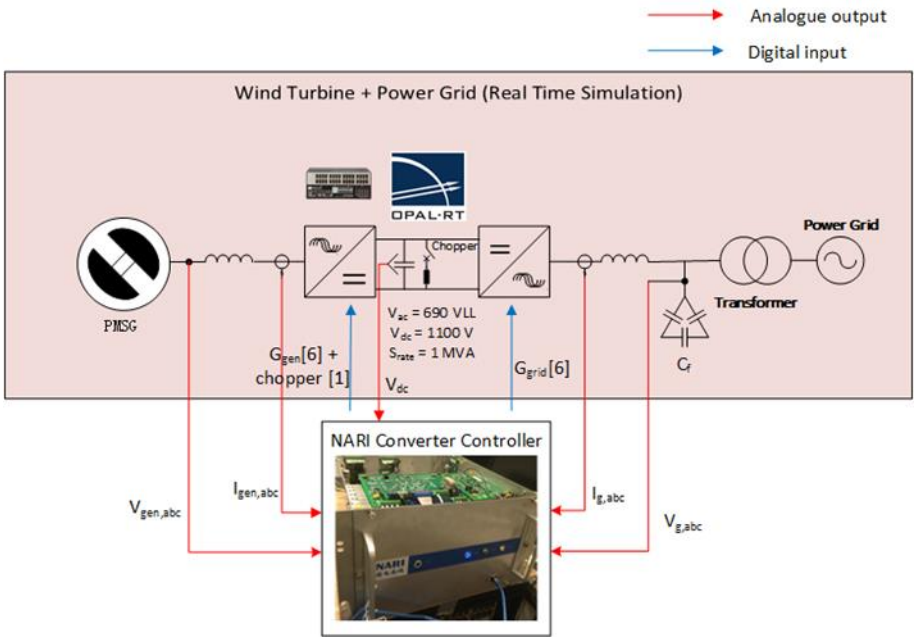

Figure 3-2: CHiL setup for the WTG controller replica input-impedance measurement

3.3 WTG INPUT IMPEDANCE MEASUREMENT IN DQ FRAME

A simplified current perturbation PHiL setup is shown in Figure 3-3. Firstly, the perturbation frequency f_{pert} is generated with the sinusoidal waveform for a wide set of individual frequency points. The established method allows an independent measurement of the *d* and *q* component of the DUT's input impedance, as presented in detail in the PROMOTioN Deliverable D16.5 [1].

This project has received funding from the European Union's Horizon 2020 research and innovation programme under grant agreement No 691714.

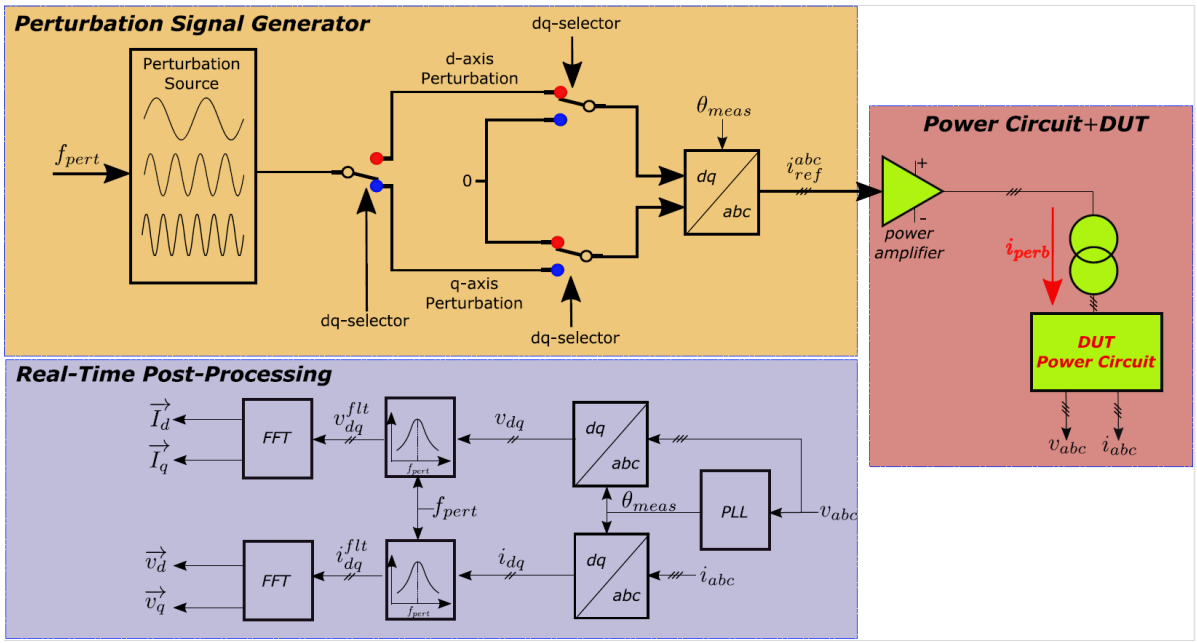

Figure 3-3: Perturbation signal generator and real-time post-processing

The inverse-park transformation is applied to generate the three-phase current reference signals $i_{\mathrm{ref}}^{\mathrm{abc}}$, which are fed into the amplifier's digital input to generate the three-phase current perturbation signals i_{perb} (see Figure 3-3). The perturbation current is then injected into the DUT circuit which excites the three-phase current and voltage at the point where the impedance measurement is conducted. The real-time post-processing block is then used to extract the magnitude and angle of a given set of current and voltage perturbations in the dq-frame. A measurement PLL is created to establish the dq-frame used for the measurement with sufficient low bandwidth so that the perturbation on the voltage caused by perturbation injection will distort the θ_{meas} output. When the θ_{meas} is determined, the current i_{abc} and voltage V_{abc} are transformed into their dq-frame counterparts (i.e. i_{dq} and v_{dq}). A bandpass filter at the perturbation frequency f_{pert} is applied to i_{dq} and v_{dq}, so that the frequency of interest can be extracted and the noise near the perturbation frequency can be rejected, which results from the frequency leakage effect of the other frequency component or simply ambient noises. The filtered dq-frame current $i_{\mathrm{dq}}^{\mathrm{flt}}$ and voltage $v_{\mathrm{dq}}^{\mathrm{flt}}$ are then fed into an FFT block, which performs the averaging on the perturbed frequency and extracts its magnitude and angle information.

3.4 RESULTS AND ANALYSIS

In this section, the input-impedance measurement results are shown and discussed. The legend is firstly explained in the following:

- PHiL - indicates the input-impedance results obtained from the physical 1-MW power converter measurement setup given in Figure 3-1.
- CHiL - indicates the input-impedance results obtained from the CHiL measurement setup given in Figure 3-2.

This project has received funding from the European Union's Horizon 2020 research and innovation programme under grant agreement No 691714.

- PSCAD - indicates the input-impedance results that are obtained from the PSCAD model.
- LC - indicates the input-impedance results obtained from the CHiL measurement setup considering only the passive output filter circuit (i.e. converter side inductor and filter capacitor)

As the measurement of the input-impedance is performed in the dq-frame, four elements are obtained by two independent measurement. Figure 3-4 and Figure 3-5 are the diagonal elements of the measured input-impedance in PHiL setup, CHiL setup and PSCAD simulation. The measurement is performed in linear space between 1.5 Hz up to 2500 Hz with 100 measurement points. Between 1.5 Hz and 1000 Hz, the PHiL results and CHiL results show good match not only for the magnitude but also for the phase angle. Beyond 1000 Hz, the PHiL results reduce quickly to below -20 dB whilst the CHiL and the PSCAD results stay close to -20 dB without sharp decline. The difference can be explained by the skin-effect and high frequency behaviour of the physical circuit that is different from its fundamental frequency electrical value (i.e. inductance and capacitance).

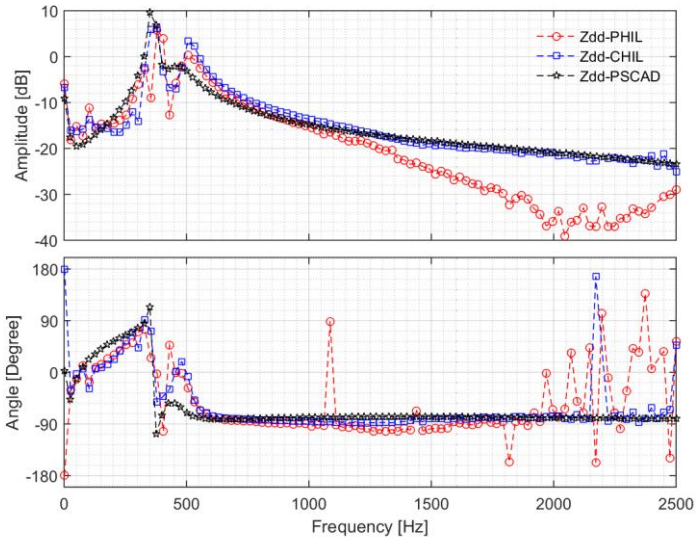

Figure 3-4: Impedance measurement results comparison - Z_{dd} full range 2500 Hz

This project has received funding from the European Union's Horizon 2020 research and innovation programme under grant agreement No 691714.

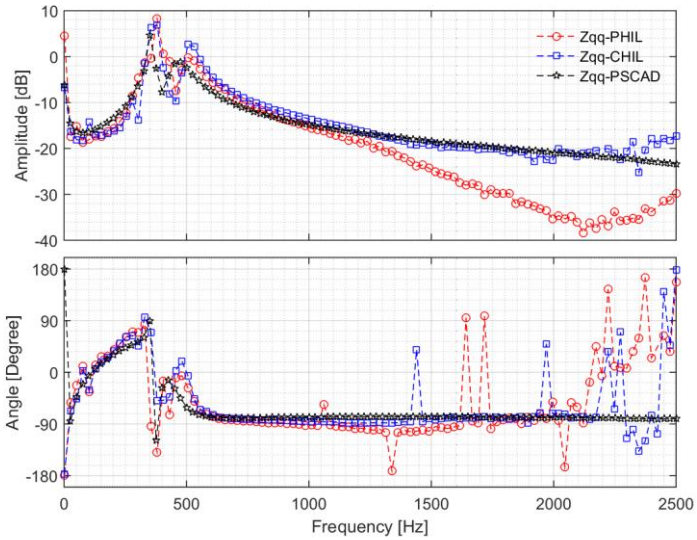

Figure 3-5: Impedance measurement results comparison - Z_{qq} full range 2500 Hz

Figure 3-6 and Figure 3-7 show the non-diagonal elements of the measured input-impedance. Both PHiL and CHIL phase angle measurement experience high uncertainty above 1000 Hz due to the low magnitude component in the cross-coupling terms (i.e. d axis couples to the q axis and vice versa). Between 200 Hz and 600 Hz, two resonance points are captured by all three measurements albeit difference in the damping near the resonance points.

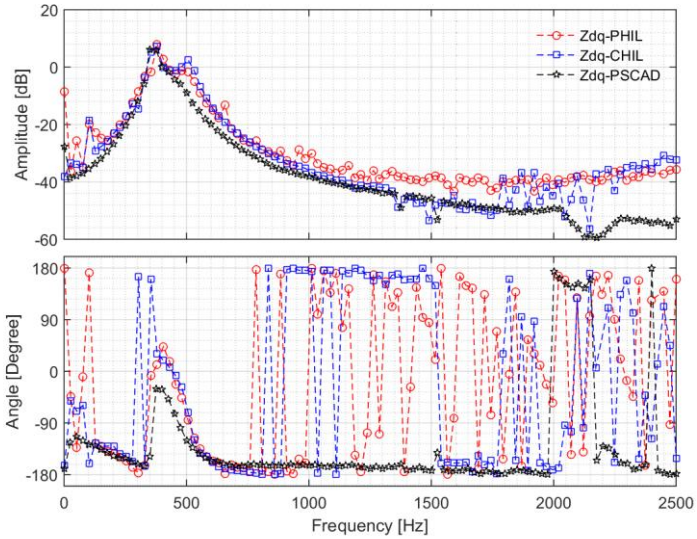

Figure 3-6: Impedance measurement results comparison - Z_{dq} full range 2500 Hz

This project has received funding from the European Union's Horizon 2020 research and innovation programme under grant agreement No 691714.

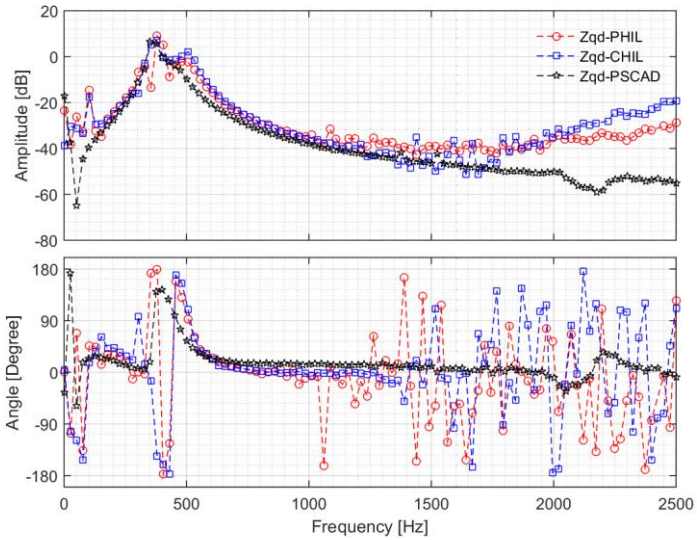

Figure 3-7: Impedance measurement results comparison - Z_{qd} full range 2500 Hz

Figure 3-8 and Figure 3-9 show the zoom-in plots for the frequency range between 200 Hz and 600 Hz of the diagonal elements of the input-impedance measurement. The passive output LC filter of the WTG is also included to showcase the control effect on the shaping of the input-impedance of the WTG. Two resonance points are the result of the passive LC resonance points + the WTG control effect cross-modulated in the *dq*-frame, hence 100 Hz separation of these two resonance points. It is clearly visible that the control effect of the WTG damped the original two resonance points of the LC passive output filter in the *dq*-frame. However, the damping effects are different between PHiL/CHiL setup and PSCAD simulation. In sum, the input-impedance measurement results from PHiL and CHiL have close matching whilst the results from PSCAD falls far from both the CHiL and PHiL setup results. The reason is likely attributed to different controller setting and the passive component equivalent series resistance choice.

This project has received funding from the European Union's Horizon 2020 research and innovation programme under grant agreement No 691714.

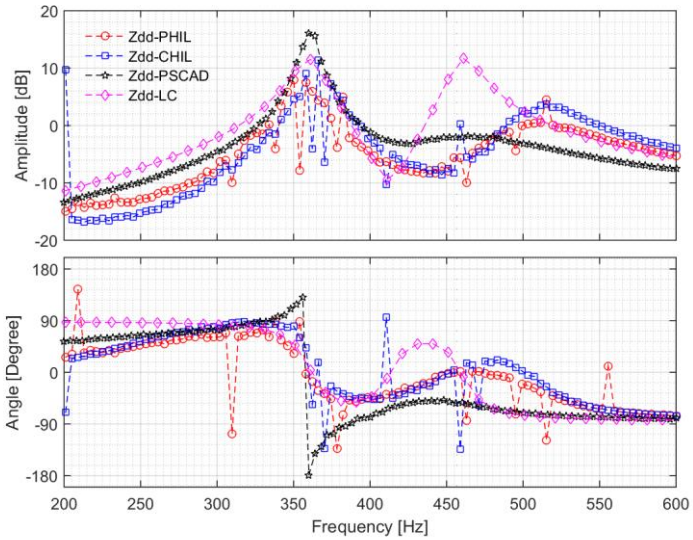

Figure 3-8: Impedance measurement results comparison - Z_{dd} mid range 200 Hz to 600 Hz

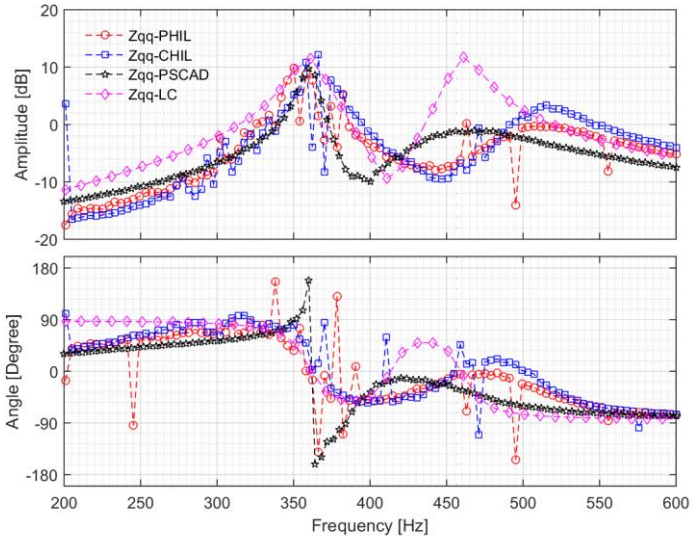

Figure 3-9: Impedance measurement results comparison - Z_{qq} mid range 200 Hz to 600 Hz

Figure 3-10 and Figure 3-11 demonstrate the zoom-in plots for the non-diagonal elements of the input-impedance measurement. In this frequency range, the cross-coupling terms are still strong enough (i.e. above -20 dB), therefore the phase angle results suffer less from the measurement uncertainty. It is clearly visible that the CHiL and PHiL results follow each other closely, whilst the PSCAD results deviation start from 450 Hz for the magnitude and from 350 Hz for the phase angle.

This project has received funding from the European Union's Horizon 2020 research and innovation programme under grant agreement No 691714.

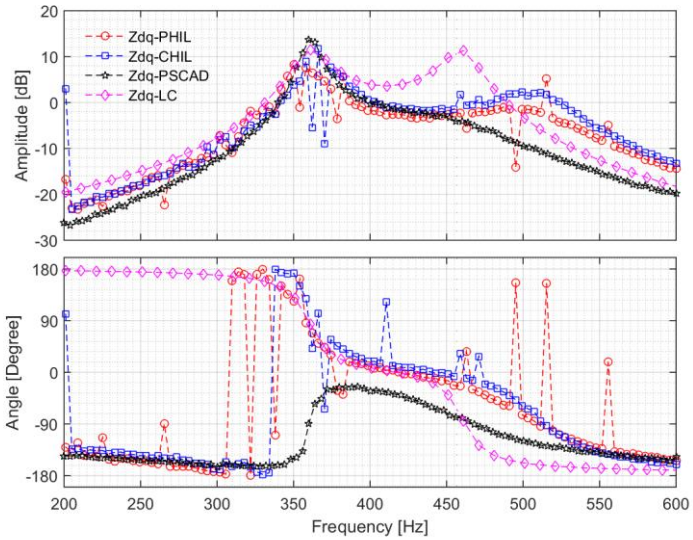

Figure 3-10: Impedance measurement results comparison - Z_{dq} mid range 200 Hz to 600 Hz

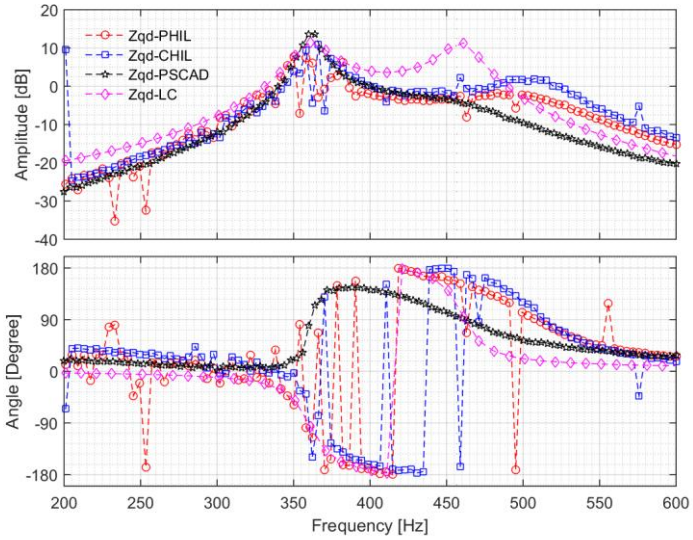

Figure 3-11: Impedance measurement results comparison - Z_{qd} mid range 200 Hz to 600 Hz

3.5 DISCUSSIONS

In this work, a current perturbation input-impedance measurement setup is established at DNV GL's FPGL. The presented measurement results confirm that the small-signal AC current perturbation method is feasible for the input-impedance measurement. Furthermore, the proposed PHiL current perturbation source does not have to match the DUT rating, making it feasible to apply the method for the input-impedance measurement of the growing offshore wind turbine generators in full power rating. Compared to the input-impedance measurement in the PHiL setup, the results from the CHiL setup are verified and considered adequate when an identical set of vendor

This project has received funding from the European Union's Horizon 2020 research and innovation programme under grant agreement No 691714.

specific controller settings are applied. In the CHiL setup, the perturbation signal is directly applied in the RTS model. Hence it is immune to sensor measurement error, scaling errors and ambient noises. The input-impedance measurement in the PSCAD is severely deviating from the PHiL and CHiL results. The reasons for such significant deviation can be attributed to the different control parameter settings as well as the choice for the equivalent series resistance in the model.

From the limited cases performed, it can be seen that the results of CHiL and PHiL are rather similar under 1000 Hz; due to the significantly less complicated test requirement of CHiL, this method can be applied industry-wide for the input impedance measurement. As PHiL's performance is less satisfactory in the high frequency range, a more suitable validation approach can be real field measurements.

This project has received funding from the European Union's Horizon 2020 research and innovation programme under grant agreement No 691714.

4 MMC INPUT IMPEDANCE MEASUREMENT AND VALIDATION

4.1 OVERVIEW

Converters such as modular multi-level converters (MMCs) and their control system can potentially interact with other active components as well as the grid impedance. In WP 16 of PROMOTiON this phenomenon is investigated and referred to as harmonic resonance analysis. Within the work package, MMC models are developed in the frequency domain to investigate potential interactions by the impedance-based approach which applies frequency-dependent impedance models of two systems and assesses potential interactions by means of classical control theory tools such as Nyquist criterion or phase and gain margins obtained from Bode plots. Analytical models have been described in deliverable D16.5 of PROMOTioN [2]. However, analytical models have been disadvantageous when representing MMCs with pre-existing control schemes not being developed according to the analytical model. So far, analytical models neglect certain control loops that are considered not being relevant for the scope of investigations. In addition, neglecting certain control loops needs to be carefully revaluated for every MMC under investigation [14], [15] [16] [17]. As a result, adapting analytically derived MMC models for analysing MMCs with pre-existing control systems has proven to be difficult and requires additional modelling effort if the model is not derived for the MMC under investigation. Furthermore, analytical models of the MMC with respect to its control system cannot be applied for investigating the influence of the controllers when the control system is black-boxed and the exact specifications of the system under investigation are unknown. Thus, black-boxed models cannot be applied which are often provided when intellectual property is a concern. Hence, the work package's objective with respect to the MMC input impedance is the following:

- Establish and validate a method which can be applied to power converters with pre-existing and/or black boxed control systems. The method has to be both applicable for simulated converter circuits as well as physical test benches.
- Compare and analyse impedances of simulated converters and those of physical converters such as the MMC Test Bench

Consequently, D16.3 shows impedance models based on a measurement-based approach for obtaining the converter impedance models whose applicability is independent of the converter under investigations. In addition, the method is applied to a laboratory scaled MMC Test Bench system as well as an equivalent time domain MMC model implemented in Matlab/ Simulink. Both simulated and physical MMCs share the same control system with differences only at the lower levels. In this report, frequency-dependent impedance models of grid-forming and grid-following control are determined.

4.2 METHOD

Figure 4-1 shows the method used for measuring the impedance of a DUT. This method is used for measuring the impedance of the MMC Test Bench and its equivalent models in positive and negative sequence [18]. The method uses the voltage or current injection approach often used when measuring impedances of power

This project has received funding from the European Union's Horizon 2020 research and innovation programme under grant agreement No 691714.

electronic components. However, the method developed in WP 16 of PROMOTioN implements the perturbation approach and Fourier analysis in real time so that only the computed impedance data needs to be saved with low sampling rate. Thus, no high resolution voltage and current measurement data for further post processing is required compared to other frequency scanning methods [19], [20], [21]. Other methods measuring impedances online or in real time, focus on identifying the grid impedance and apply analytical converter models [22], [23]. In addition, impedances are measured in the dq-frame and are dependent on the grid angle which has to be consistent for the grid and converter impedance [24], [23]. This makes the separation of grid and converter modelling difficult which is needed apparent impedance analysis when grid and converter models are provided by different entities. Other methods inject a wide-band or multi-tone frequency resolution and power spectrum signal for measuring the frequency response [25], [26]. This approach is valid for measuring the grid impedance. However, measuring the impedance of active components such as MMCs simultaneously for different frequencies imposes additional uncertainties in the measurements because the converter reactions cannot be easily related to distinct frequencies. While allowing very short time durations for the measurements, a trade-off for accuracy has to be made [26]. Hence, the measuring method developed in PROMOTioN is based on a hybrid approach. The method subsequently injects perturbation frequencies similar to other frequency scanning method for best accuracy while on the other hand the method is implemented offline (simulations) or in real-time when physical components are coupled.

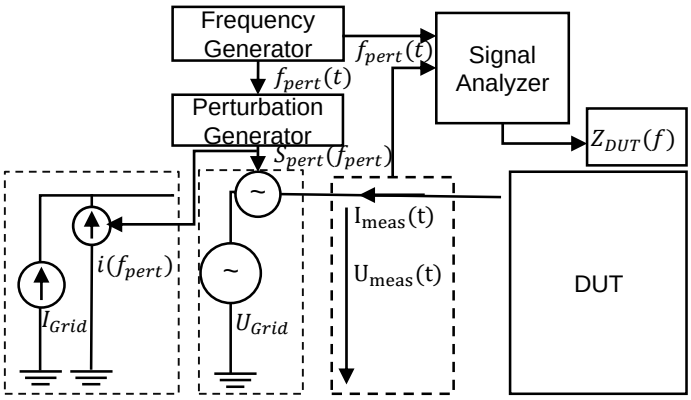

Figure 4-1:Impedance measuring method [18]

This method determines the impedance of the MMC, or device under test (DUT) online, while measurements are taken so that no large data files with high sampling rates need to be recorded for further post-processing such as Fourier transformation. As shown in Figure 4-1, a perturbation frequency signal $f_{pert}(t)$ is created by the frequency generator and subsequently fed into the perturbation generator and the signal analyser. As perturbation signals, a current perturbation or voltage perturbation can be used. Depending on the perturbation source, the sinusoidal output signal $S_{pert}(f_{pert})$ of the perturbation generator is used as input for a current source with $I = I_{pert}(t)$ or a voltage source with $U = U_{pert}(t)$. An additional current source or voltage source at grid frequency sets the grid operation point. The signal analyser calculates the frequency-dependent impedance $Z_{DUT}(f)$ of the DUT with $f = f_{pert}(t)$ on the basis of the terminal measurements $U_{meas}(t)$ and $I_{meas}(t)$. This method is implemented in Matlab/Simulink and adapted for real-time simulations with RT-Lab [18].

This project has received funding from the European Union's Horizon 2020 research and innovation programme under grant agreement No 691714.

4.3 TEST CASES

The test case 2.3.2 “Unit MMC Converter Model Validation for Resonance Phenomena Studies” is used as basis for setting up the following test cases [27]. The goal of test case 2.3.2 is to validate impedance models of the MMC Test Bench Laboratory at RWTH Aachen University. The test cases aim to verify the frequency domain results with time domain simulations and laboratory measurements with respect to MMCs operating in different operation modes. Figure 4-2 shows exemplarily an HVDC circuit connecting offshore wind turbines with the AC onshore grid. Two test cases are conducted in within this chapter with respect to MMCs. Test case A addresses the ac side impedance of a MMC operating in grid following control and test case B in grid forming control mode. The input impedance of the offshore wind turbine is studied in chapter 4.

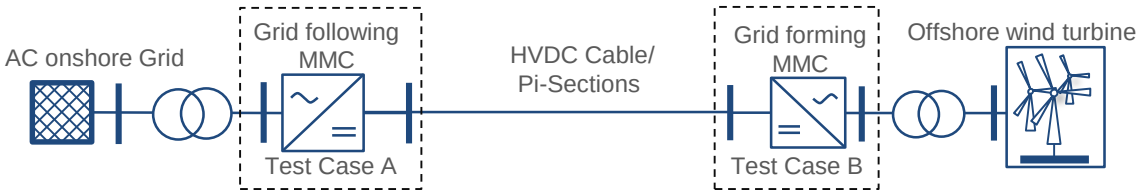

Figure 4-2: MMC test cases

The specifications of the MMC Test Bench and the parameters of the equivalent time domain model can be found in Table 2-1 to Table 2-3. Table 4-1 shows the set points for the conducted test cases. The impedance measurements for MMC 1 operating in grid following (test case A) and grid forming control (test case B) are executed one after another with MMC 2 always controlling the DC voltage as explained in the following section. When operating in grid forming control, a current source is connected to MMC 1 feeding an active power of P_{AC} = 0.5 p.u. to establish a controlled working point.

Table 4-1: MMC impedance measurement set points for test case A and B

	TEST CASE A MMC 1: GRID FOLLOWING		**TEST CASE B MMC 1: GRID FORMING**	**MMC 2**	
Controlling Mode	P	Q	V_{AC}	V_{DC}	Q
Reference value [p.u.]	0.5	0	1	1	0

4.4 POWER HARDWARE SETUP

Figure 4-3 shows the power hardware setup to measure the MMC Test Bench impedance. It can be divided into two parts, the power hardware part (*MMC Test Bench*) and the simulated part (*Real-Time Simulation*). The MMC Test Bench uses two MMCs connected by PI sections on the DC side. Y-D transformers transform the grid voltage supplied by the power amplifiers from 208 V to 400 V as required by the converters. The real-time simulation is coupled with the MMC Test Bench through analogue input and output ports transmitting control signals and receiving measurements as voltages signals between $u_{ctrl} = [-10\,V;\ 10\,V]$. The power amplifiers amplify the

This project has received funding from the European Union’s Horizon 2020 research and innovation programme under grant agreement No 691714.

voltage signals received from the RTS. Depending on the test case, PA 1 sets either a three-phase voltage U_1 (test case A) or feeds in a three-phase current I_1 (test case B) according to the variable frequency signal $S(f)$ coming from the frequency generator. The voltage U_1 consists of the grid voltage at grid frequency superimposed by the variable frequency perturbation voltage. In case of a current infeed, a grid and perturbation current I_1 is fed into the test circuit by PA 1. The control signals at PA 2 translate into the grid voltage U_{Grid} for both test cases. For converters in grid forming control operating the power amplifier as current source instead of voltage source is necessary because in grid forming control the voltage is defined by the converter instead of the grid.

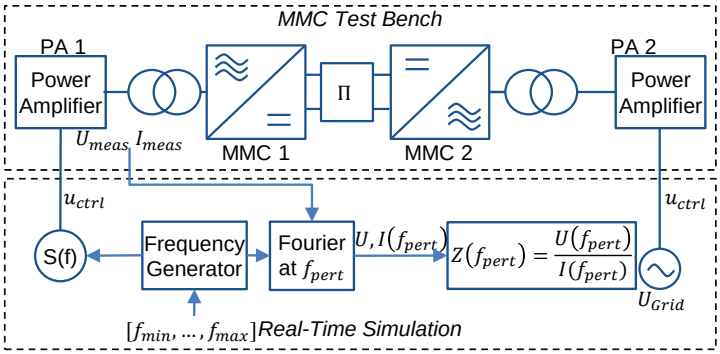

Figure 4-3:Offshore MMC Test Bench impedance measurement setup

The measured signals comprise of the voltage signals U_{meas} and the current signals I_{meas} measured at the terminal of PA 1. The signals are processed by real-time by Fourier analysis over a running window calculating the voltage and current share at perturbation frequency, f_{pert} provided by the frequency generator. The resulting voltage $U(f_{pert})$ and current $I(f_{pert})$ at f_{pert} determine the frequency-dependent impedance $Z(f_{pert})$ of the MMC Test Bench.

The power hardware setup for measuring a single MMC impedance consists of an additional MMC (MMC 2) connected on the DC side so that the setup can be used for measuring the impedance of MMCs operating in different control modes. For instance, changing the control system from grid following to grid forming control, only requires to change the control mode in the real-time simulation part of the setup and not in the MMC Test Bench.

4.5 OFFLINE SIMULATION SETUP

Figure 4-4 shows the offline simulation setup. The setup is equivalent to the MMC Test Bench setup presented Figure 4-3 with the exception that the MMC circuit is simulated in Matlab/Simulink and the measurement method is directly connected to the model as no power amplifiers are needed for simulations. A one capacitor model, representing the MMC submodules as one voltage source per arm is used for simulating the electrical part of the MMC.

This project has received funding from the European Union's Horizon 2020 research and innovation programme under grant agreement No 691714.

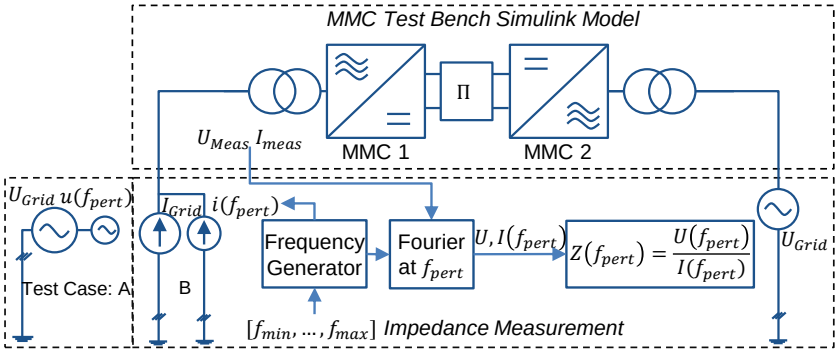

Figure 4-4:Offshore MMC simulation mode impedance measurement setup

Similar to the power hardware setup, the offline simulation setup uses current sources instead of voltage sources when MMC 1 is operating in grid forming control.

4.6 COMPARISON BETWEEN OFFLINE SIMULATION AND POWER HARDWARE MEASUREMETNS

Figure 4-5 shows the measured impedance of the MMC Test Bench and the simulated MMC in grid following control mode in positive and negative sequence and Figure 4-6 shows the measured impedance for the MMC in grid forming control.

It is shown that both for grid forming and grid following control mode at low frequency, the positive sequence impedance differs from the negative sequence impedance while at frequencies above 1 kHz the frequency response in positive and negative sequence both shows inductive behaviour with additional resistive damping above 1100 Hz. Additionally, the results indicate that above the fundamental frequency, the frequency behaviour is dominated by the control system, as the magnitude and phase of the measured impedances differs significantly when the control system is operated in different modes. Starting at 800 Hz the impedances show identical frequency behaviour indicating that the passive components, in particular inductive parts highly influence the MMCs' impedance. At fundamental frequency, a sharp peak can be observed in the measurements. The peak is caused by the fact that at 50 Hz, the operating point of the MMC dominates the impedance response. According to the set points given in Table 4-1, the converter provides active power at fundamental frequency of 50 Hz. As the perturbation source and grid voltage and current have the same frequency, the measured converter response cannot be distinguished anymore from the operating point and therefore, should not be considered as a resonance point. A similar behaviour at fundamental frequency can also be observed in analytical models [14], [17].

This project has received funding from the European Union's Horizon 2020 research and innovation programme under grant agreement No 691714.

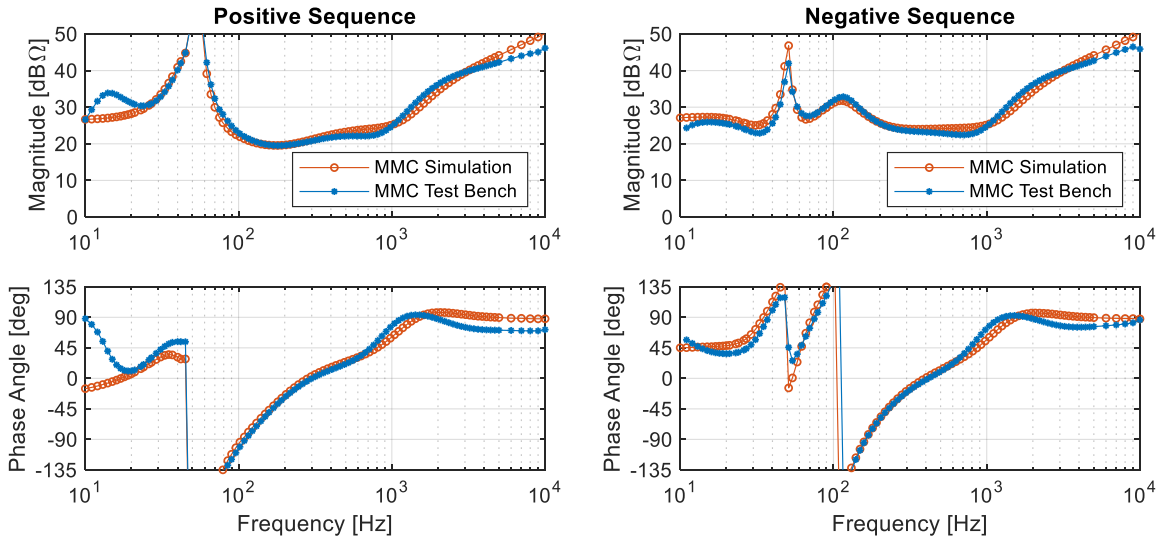

Figure 4-5:Impedances grid following MMC Test Bench and simulation

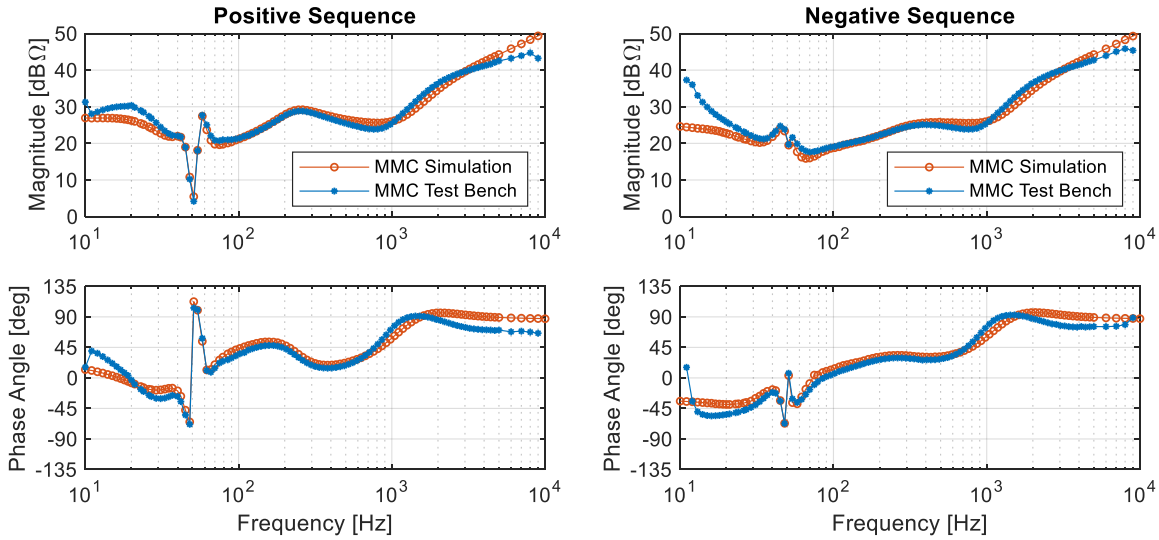

Figure 4-6: Impedances grid forming MMC Test Bench and simulation

It can be seen that the impedances of simulated MMCs match the impedances of the MMC Test Bench in areas where the frequency behaviour is mainly influenced by the control systems. At high frequencies, the impedance of the simulated MMC and of the MMC Test Bench have both inductive behaviour. However, the MMC magnitude of the MMC Test Bench impedance shows higher damping. This effect can be contributed to the fact that the passive components such as the arm inductances dominate the frequency behaviour at high frequencies. The results further indicate that the specified parameters of the passive components applied on the simulated MMC do not exactly match the real physical values. At low frequencies, the impedance of the MMC Test Bench differs significantly from that of the simulated MMC, e.g. a resonance peak between 10 Hz and 20 Hz, which is not present in the simulated results, is observed in the positive sequence impedance of the MMC Test Bench. These low frequency resonances can be contributed to internal MMC dynamics caused by the internal circulating current

This project has received funding from the European Union's Horizon 2020 research and innovation programme under grant agreement No 691714.

and can be seen in other MMC responses [16]. The results indicate that the model used for simulating the electrical part of the MMC is not able to accurately represent the low-frequency characteristics of the MMC that are present for the MMC Test Bench. Further tests will aim at narrowing down observed differences in the results by applying more detailed time-domain MMC models. In addition, comparing the results with impedance measurements of the MMC Test Bench in open loop operation will further give insights about the impact of the control system and the influence of the electrical part of the converter on the frequency behaviour.

4.7 CONCLUSION

The presented method can be both applied for measuring the frequency-dependent impedance of simulated MMCs as well as for a laboratory setup such as the MMC Test Bench. The method is applicable for measuring the frequency response of MMCs with various control systems when an analytical derivation of the converter impedance is not feasible. The impedances of MMCs in grid following and grid forming controls can be measured requiring either a voltage source or current source perturbation. The results show that the MMC's impedance can be measured by means of a simulated MMC model depending on the frequencies of interest. Attention should be made when investigating sub-synchronous resonance phenomena by means of the simulated MMC models because it is shown that below the fundamental frequency, the frequency response of the simulated MMC differs significantly from the one of the MMC Test Bench. Further studies also need to be carried out to investigate the effect of the transformer impedance, in particular at high frequencies in the kHz range because higher damping can be seen in the MMC Test Bench impedance.

This project has received funding from the European Union's Horizon 2020 research and innovation programme under grant agreement No 691714.

5 BLACK-START OF WPP

5.1 INTRODUCTION

In recent years, with increasing penetration of wind power in the electrical network, and the corresponding reduction of conventional generation plants, there is interest from transmission system operators (TSOs) in procuring black start services from wind power plants. Furthermore, offshore wind turbine generators (WTGs) with the capability of starting, self-sustaining, and energising its own offshore AC network offer benefits of flexibility and cost savings to wind power plant operators in the event of prolonged outages of the export connection.
The WTG dynamic performance depends on several coupled systems, namely aerodynamics, structural dynamics, and WTG pitch and torque control as well as electrical dynamics, as shown in Figure 5-1. Therefore, a complete assessment of WTG performance involving of all four of these systems is recommended prior to the application of the technology.

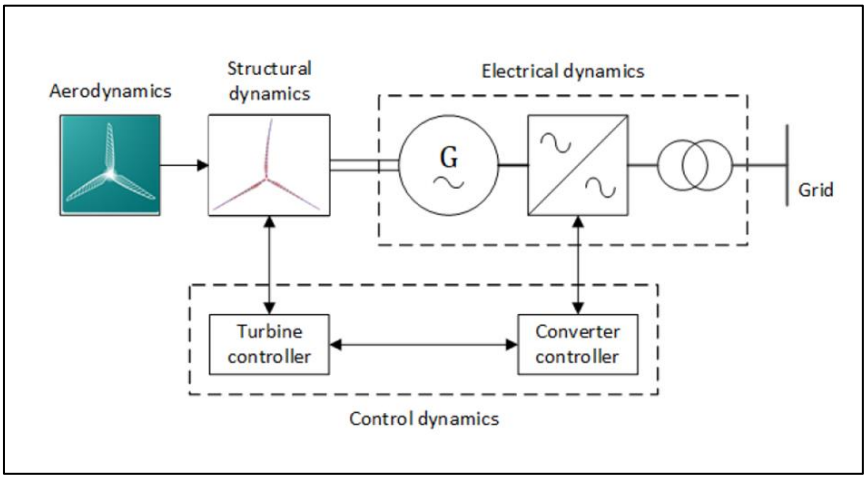

Figure 5-1: Wind turbine dynamic model coupled systems.

A real time co-simulation platform which integrates a Bladed WTG aero-elastic model with RT-LAB (based on Simulink) electrical dynamic models is proposed as a validation tool. This chapter presents two test bench configurations which integrate the co-simulation and hardware-in-the-loop (HiL) methodologies. The test benches are used for development and validation of self-energisation and black start capability of a 1-MW Type 4 WT.
The test bench capability can be extended to any test case which involves coupling between WT and electrical system dynamics, such as low voltage ride through (LVRT), fast frequency response, inertial response or operation in an islanded network.

This chapter will describe the control aspects to be investigated for the self-energisation and black start capability of a WT. The test benches used for the development and validation of such functionality will be introduced. The study case is defined together with the energisation strategies to be tested. Finalising with the results of test cases and main conclusions of the experimental validation.

This project has received funding from the European Union's Horizon 2020 research and innovation programme under grant agreement No 691714.

The test case that is intended to be reproduced is the self-energisation of a 1-MW WTG that belongs to a string of wind turbines in a wind plant, as depicted in Figure 5-2.

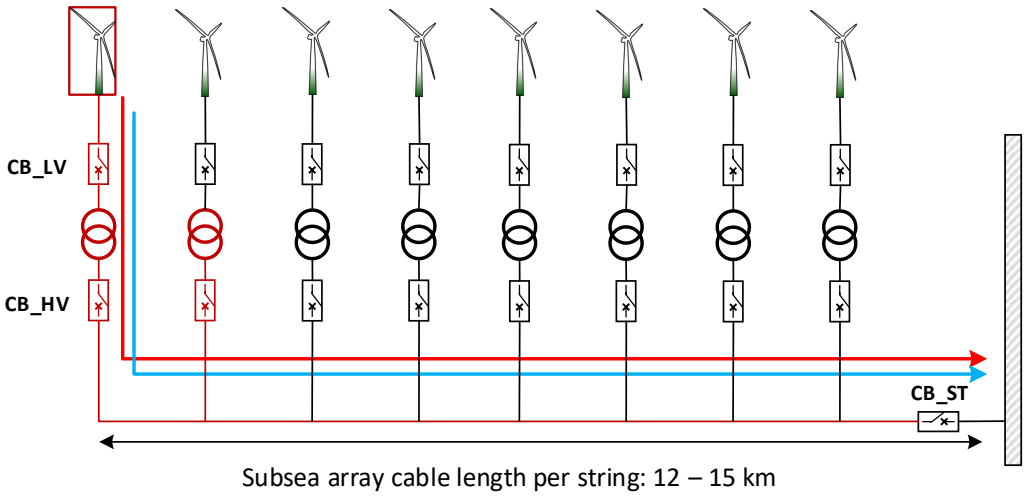

Figure 5-2: String of wind turbines in a wind power plant.

The energisation includes the wind turbine transformer, the auxiliary loads of the wind turbine, the HV cable and a second wind turbine transformer. All the mentioned components are highlighted in red in Figure 5-2.

There are two operational approaches to energise the proposed power circuit. The first one is known as soft energisation and the other one as traditional hard energisation. Both are explained in detail in the following sections.

Soft energisation

Soft energisation is referred when the loads/equipment to be energised are already physically connected before applying any voltage. From Figure 5-2, CB_LV and CB_HV are closed before forming a voltage in the grid-side terminal of the converter. This approach helps on reducing the transient voltage due to the inrush current when energising the equipment, in this case the inrush current of the two transformers to energise.

For the soft energisation of the circuit, the main consideration is that the converter has enough power input from the generator to supply the required reactive power needed by the loads, transformers and HV cable. This means that the converter controller on the generator side, grid side and the DC bus control need to be carefully designed to maintain the balance of power between the generator and grid side.

Soft energisation has been studied and tested with traditional generation by DNV GL and TenneT [28].

Hard energisation

Hard energisation refers to the traditional approach to energise a certain segment of a network by switching in by sections the circuit to be energised. This method entails higher voltage transients that can be difficult to control and higher dielectric stress in the equipment [28].

This project has received funding from the European Union's Horizon 2020 research and innovation programme under grant agreement No 691714.

For the proposed study case, it would mean that CB_LV is closed and CB_HV is open before any voltage is built by the converter. Once the converter has built the voltage in its transformer and auxiliary loads, the CB_HV is closed to energise the rest of the power circuit. When the CB_HV is closed the converter will see a large current transient due to the inrush current of the HV cable but mainly the second wind turbine transformer. This transient will challenge the grid forming controls of the wind turbine converter, since the grid forming control is limited by the amount of generated power and can be pushed to instability due to the power imbalance between the generator, DC bus and grid side.

5.2 TEST SETUP

HIL methodology is used for the test benches, complemented by the co-simulation environment between Bladed and RT LAB. The proposed test benches support the different stages of development and validation of the WT functions.

- Control-Hardware-in-the-Loop (CHIL) include the models of all the electrical primary equipment of the WT and the electrical network.
- Power-Hardware-in-the-Loop (PHIL) includes only the model of the generator which is interfaced to WT converter and primary equipment through a power amplifier.

The CHIL test bench facilitates development of converter and WT grid-forming control algorithms, while the PHIL configuration enables testing of the converter in grid-forming mode using a controlled environment provided by DNV GL's Flex Power Grid Laboratory (FPGL) in the Netherlands.

5.2.1 CO-SIMULATION TEST BENCH

Figure 4-3 shows an overview of the co-simulation platform. Bladed Hardware Test Module (BHTM) is used to provide a real-time test framework to link together various co-simulation hardware and software components. Communication between BHTM and the electrical models on the OP5700 platform is asynchronous with an update period of 10 ms. WT structural dynamics with frequencies in the order of 100 Hz are coupled with electrical dynamics with frequencies up to 29 kHz. Test case procedures are defined and executed, and results recorded, using BHTM. A proprietary Windows application, supplied by the converter manufacturer, provides an interface to the converter controller.

This project has received funding from the European Union's Horizon 2020 research and innovation programme under grant agreement No 691714.

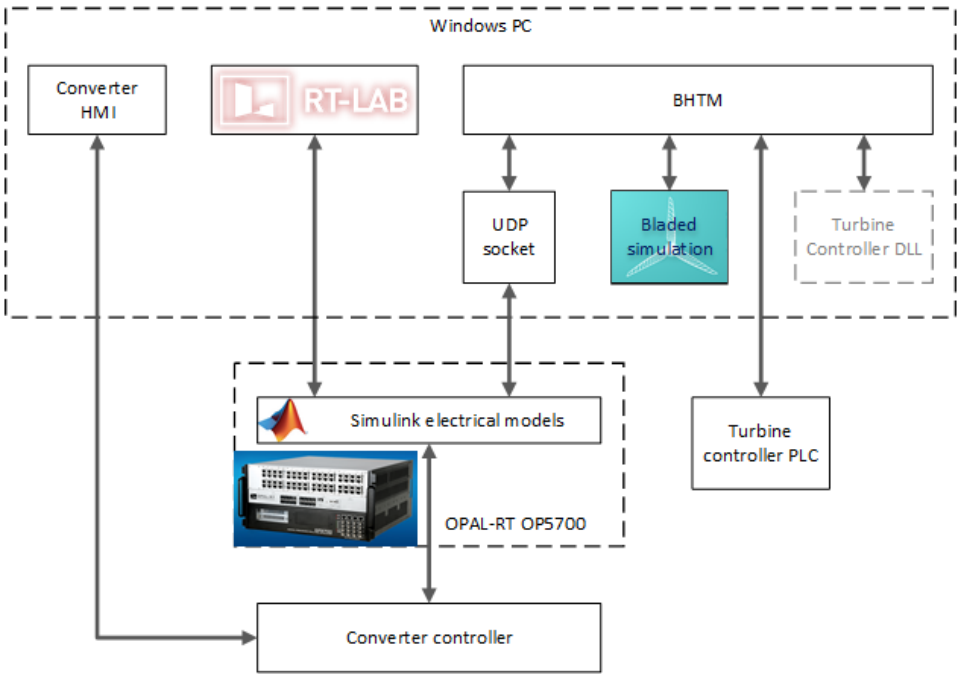

Figure 5-3: Co-simulation platform

Bladed WT model:

The WT is modelled using DNV GL's Bladed software. The model includes WT aerodynamics, multi-body structural dynamics, drive-train and pitch system. The turbine environment for each test case may include turbulent or extreme wind conditions. Bladed models are frequently used by WT OEMs for load calculations during WT design and certification processes. Load calculation models contain detailed definitions of:

- blade geometry plus physical and aerodynamic properties
- tower geometry and physical properties
- blade and tower flexibility modes
- drivetrain dynamics
- pitch actuator dynamics

For real-time simulation, the WT load calculation model was simplified to enable a simulation capable of running with a 10 ms fixed time step.

WT controller:

In the test bench, the WT controller may be implemented as a Windows DLL, or with hardware (PLC). In both cases, the turbine controller communicates with the Bladed turbine model through BHTM, and with the converter controller through BHTM and the OP5700.

The WT controller determines the operational state of the turbine. In each test case, the turbine is initially in an idling state and the WT controller then performs a start-up sequence to put the WT into a power production state. For this work, the WT control algorithm has been adapted for grid-forming operation.

This project has received funding from the European Union's Horizon 2020 research and innovation programme under grant agreement No 691714.

OPAL RT

The electrical models are implemented in Simulink, which are enabled for real-time execution by RT LAB. The models run on an OP5700 real time simulator. Digital and analogue I/O modules in the OP5700 are used to interface the converter controller in the HiL test bench.

5.2.2 CO-SIMULATION CHIL

The co-simulation CHiL test bench allows the control development/validation for the WT and converter controller using the co-simulation and HiL capability of the test bench before its deployment to the converter. Figure 5-4 shows a simplified diagram of the co-simulation CHiL test bench.

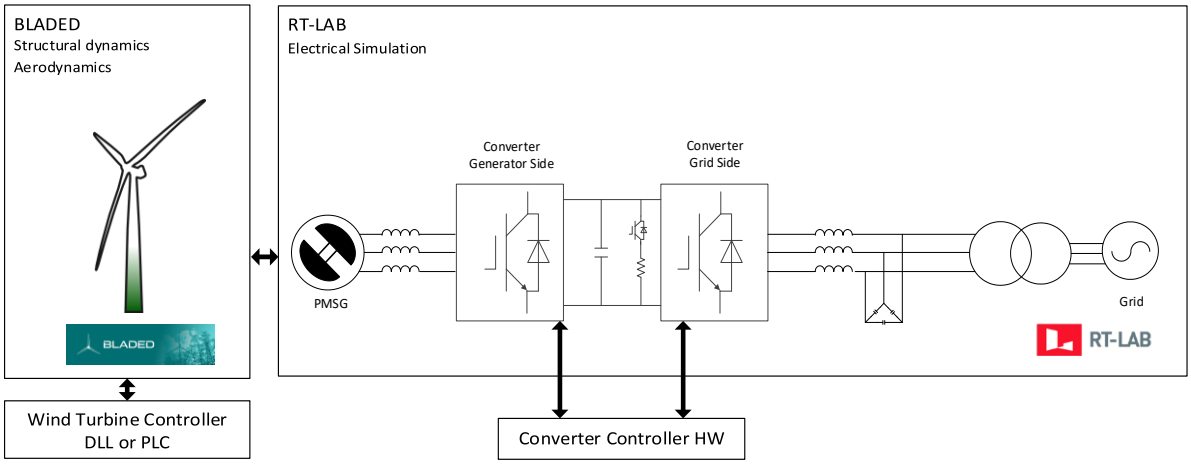

Figure 5-4: Co-simulation CHiL test bench.

For the black start validation, the electrical model includes the WTs main primary equipment. On the grid side of the converter the primary equipment reflects the devices used in power circuit (cf. Figure 5-4) of the laboratory experiment, these are further explained in the Power setup section.

The simulation runs with a fixed time step of T_s = 34 µs which is sufficiently fast to model the converter PWM switching and to simulate electrical transient events associated with MV cable charging and transformer inrush currents.

5.2.3 CO-SIMULATION PHIL

The co-simulation PHiL power amplifier emulates the generator voltage allowing a power connection to the generator side converter terminal. The turbine controller is included as either a software or hardware component. Figure 5-5depicts a simplified diagram of the co-simulation PHiL test bench.

This project has received funding from the European Union's Horizon 2020 research and innovation programme under grant agreement No 691714.

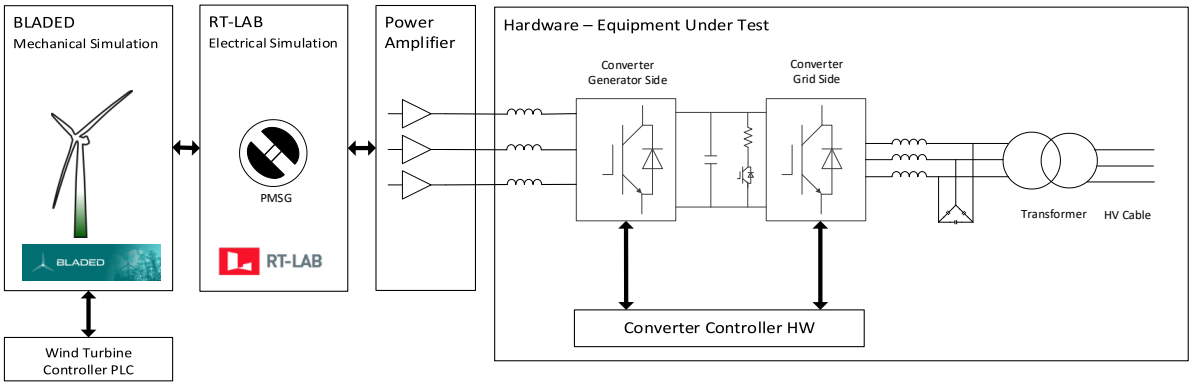

Figure 5-5: Co-simulation PHiL test bench.

The power circuit used in the laboratory is shown in Figure 5-6. The power is sourced from the power amplifier emulating the PMSG which is rated to 100 kVA. This power rating is sufficient since the circuit to be energised does not need more than 100 kVA for black start. After the power amplifier an isolation transformer is added to increase the voltage from 400 V maximum voltage sourced by the amplifier to 690 V the WT converter voltage rating.

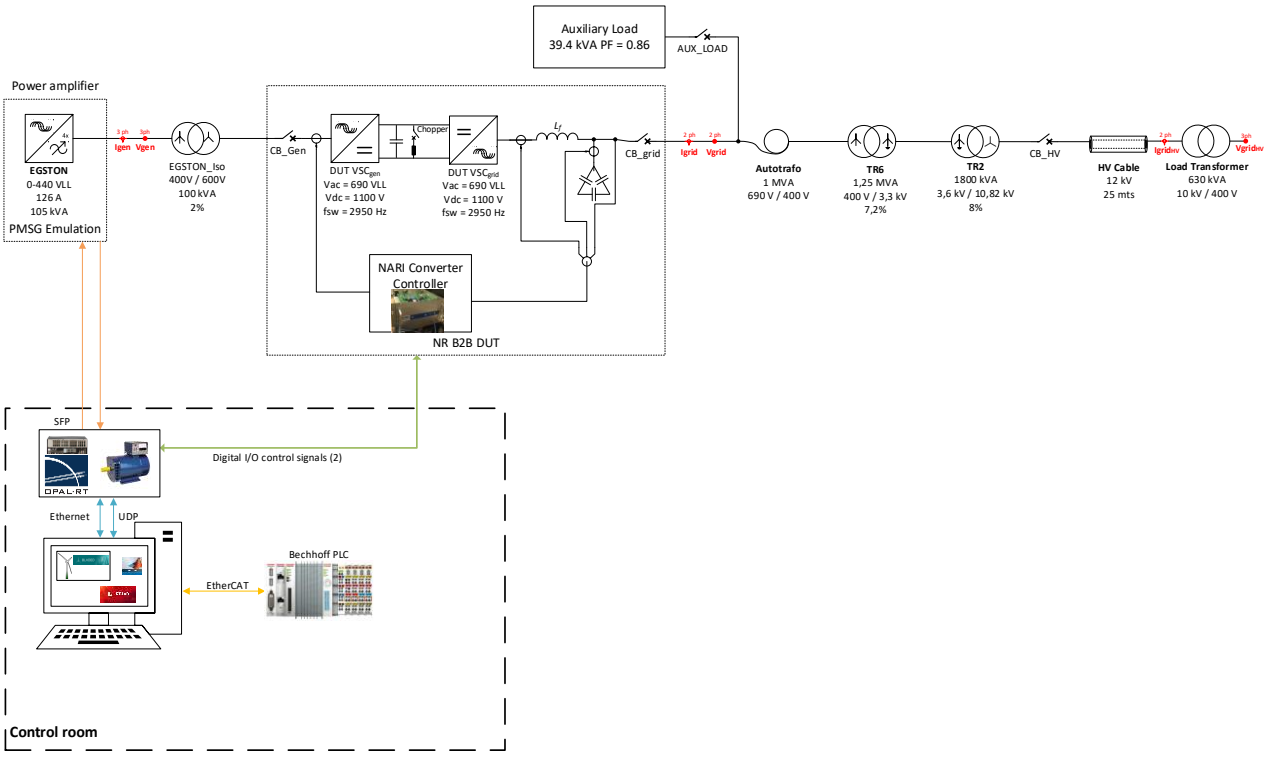

Figure 5-6: Schematic power circuit of the test bench and co-simulation

On the grid side of the WT converter a load bank to represent the auxiliary loads of the WT (39.4 kVA & PF = 0.86) is used. Later the WT transformer (1 MVA) is used to tap down the voltage from 690 V to 400 V. an additional two transformers are connected in the test circuit to aid in voltage transformation to reach 10.8 kV. The MV breaker

This project has received funding from the European Union's Horizon 2020 research and innovation programme under grant agreement No 691714.

connects the second part of the circuit, which consist of a 25 m. 50mm2 of 10.3 kV cable, and a transformer (630 kVA) to represent a transformer of a second WT.

The measurements of the power circuit are indicated by red nodes in Figure 5-6. It is important to mention for interpretation of the results, that the measurements on the test bay (grid-side measurements) obtained with a fast transient recorder are not synchronised in time with the co-simulation measurements (generator-side measurements) due to equipment limitations.

5.3 RESULTS AND DISCUSSIONS

5.3.1 SUMMARY OF TEST CASES

For the testing phase, it is necessary to test the proposed energisation approaches soft and hard, with different wind profiles. Table 5-1 contains the test cases tested in both the CHiL and the PHiL test bench. In the case of PHiL hard energisation, one case was possible to run with a co-simulation test bench and the second case only with a fixed speed of the emulated generator and no co-simulation, this is further explained in Table 5-1.

Table 5-1: Test cases in both CHiL and PHiL test bench.

Energisation strategy	Test Case Name	Conditions
Soft energisation (both CHiL and PHiL)	• DLC1-2: 5m/s, with load • DLC1-2: 12m/s, with load • DLC1-3: 12m/s, with load • DLC1-4: 7m/s, with load • DLC2-3: 12m/s, with load	All cases are run with Bladed co-simulation
Hard energisation cases for CHiL	• DLC 1-2: 12 m/s, with load	All cases are run with Bladed co-simulation
Hard energisation cases for PHiL	• DLC1-2: 12m/s, No load, GF-FRT Strategy	No co-simulation, fixed PMSG speed

Wind Conditions Specified by IEC 61400-1 Design Load Cases

DLC 1.2 – Power production with Normal Turbulence Model (NTM) at low and rated wind speeds (5 m/s and 12 m/s).

DLC 1.3 – Power production with Extreme Turbulence Model (ETM) at rated wind speed 12 m/s.

DLC 1.4 – Extreme Coherent gust with Direction change (ECD), starting wind speed 7 m/s.

DLC 2.3 – Extreme Operating Gust (EOG), starting wind speed 12 m/s.

General Acceptance Criteria

This project has received funding from the European Union's Horizon 2020 research and innovation programme under grant agreement No 691714.

The main purpose for these testing cases is to prove the overall functionality and stability of the proposed black start energisation strategies, through a soft energisation, hard energisation and a hard energisation using GF-FRT. The generic acceptance criteria to evaluate the test results is to be able to build a voltage in the secondary winding of the load transformer as per the power circuit diagram (see e.g. Figure 5-6 in case of PHiL).

5.3.2 CHIL CO-SIMULATION RESULTS

Soft energisation

The soft energisation of the model of the power circuit was successfully validated for all the different wind profiles.

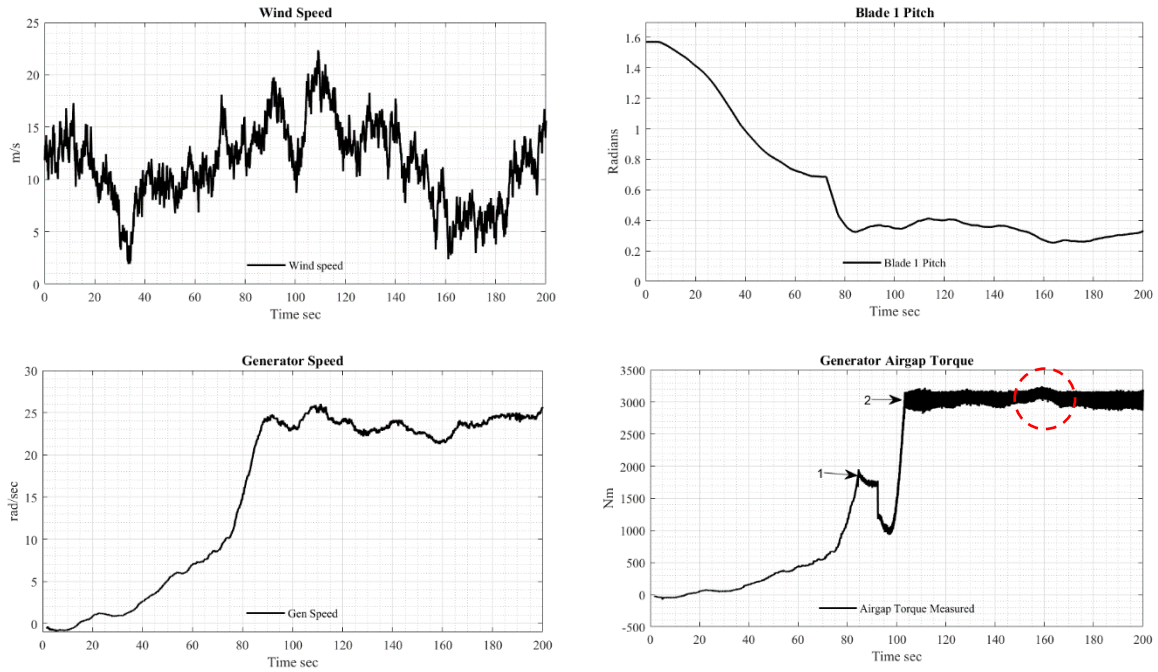

Figure 5-7: Wind speed (top left), Blade 1 Pitch(top right), Generator Speed (bottom left) and Generator Airgap Torque (bottom right) of the DLC 1-3 12 m/s test case in CHiL test bench - Soft Energisation

The results of case DLC 1-3 12m/s, with an extreme turbulence in the wind profile, show that the soft energisation was successful. The pitch control is able to maintain speed with a turbulent wind profile and do not fall in over speeding. On the generator side the speed in this test case is fluctuating more and together with the turbulence seen in the wind profile.

The generator air-gap torque is depicted in bottom right of Figure 5-7, where Arrow 1 in the figure shows when the converter starts conducting. Shortly after this the power production starts increasing the air-gap torque (Arrow 2). The effect of wind turbulence on the air-gap torque can be observed around t = 160 s (circled in red), which is also portrayed in Figure 5-8 top right.

This project has received funding from the European Union's Horizon 2020 research and innovation programme under grant agreement No 691714.

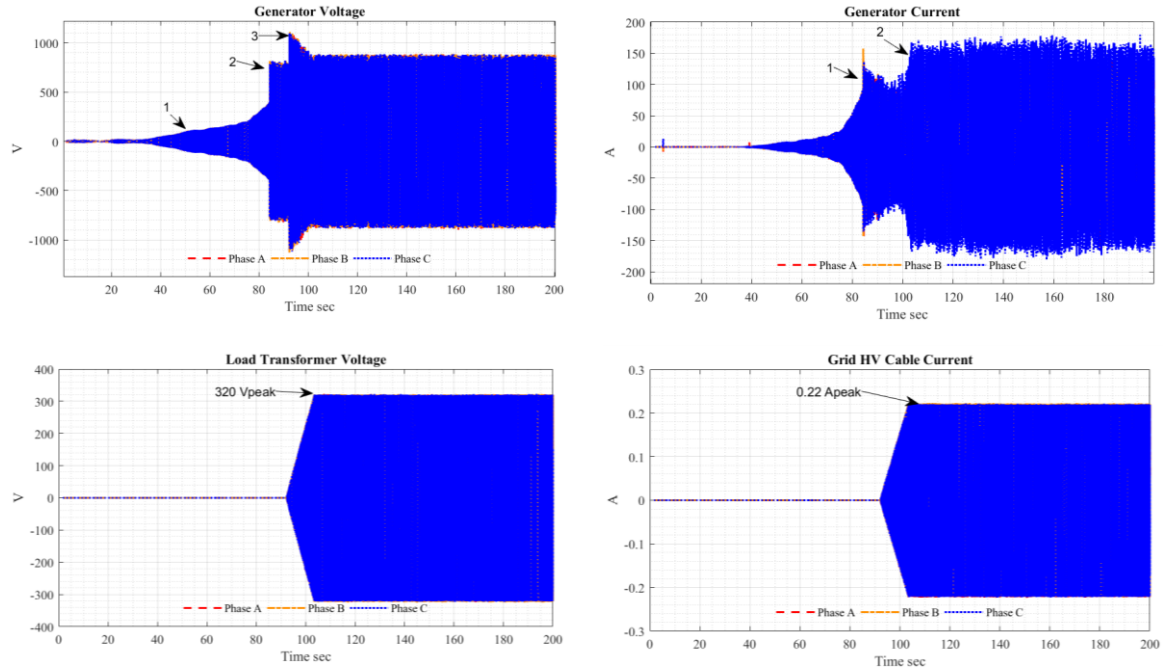

Figure 5-8: Generator voltage (top left), Generator current (top right), Load transformer voltage (bottom left) and Grid side current (bottom right) of the DLC 1-3 12 ms test case in CHiL test bench – Soft Energisation

Hard energisation

The hard energisation test case is the most challenging approach to black start the proposed power circuit for the converter controllers. The challenges come from the transient current seen by the converter controller by the inrush current of the transformers to energise. The test case of hard energisation with nominal wind conditions and nominal turbulence has been proved successful for the energisation case. Here the results for the case of DLC 1-2 12 m/s with normal turbulence in the wind speed are presented.

The start sequence is the first event in the test, the start command is given by the wind turbine controller. After the wind turbine controller waits for a confirmation that both breakers generator and grid side of the power converter have been closed before it starts accelerating the rotor. Once the breakers are closed the speed of the rotor will increase, this is done by pitching in the blades of the wind turbine, observed in top left figure in Figure 5-9. As the blades start to pitch in, the generator speed start to increase, until it reaches the nominal speed. The trend of the measured air-gap torque follows the generator speed, in the bottom right figure in Figure 5-9 at t = 98 s the generator converter side starts switching (1). The drop in the generator air-gap torque seen at t = 105 s happens since the grid side of the converter starts switching to build the voltage to a nominal value (2). Finally, the transient observed in (3) at t = 126 s occurs when the hard energisation is initiated and the load increases.

On the generator side of the converter is possible to see three main events throughout the test. First (1) indicates the ramping up of voltage as the generator speed increases. Second (2) the converter starts switching on the generator side. Third (3), the transient voltage is the transient seen due to the starting of switching on the grid side and therefore slowly ramping up voltage.

This project has received funding from the European Union's Horizon 2020 research and innovation programme under grant agreement No 691714.

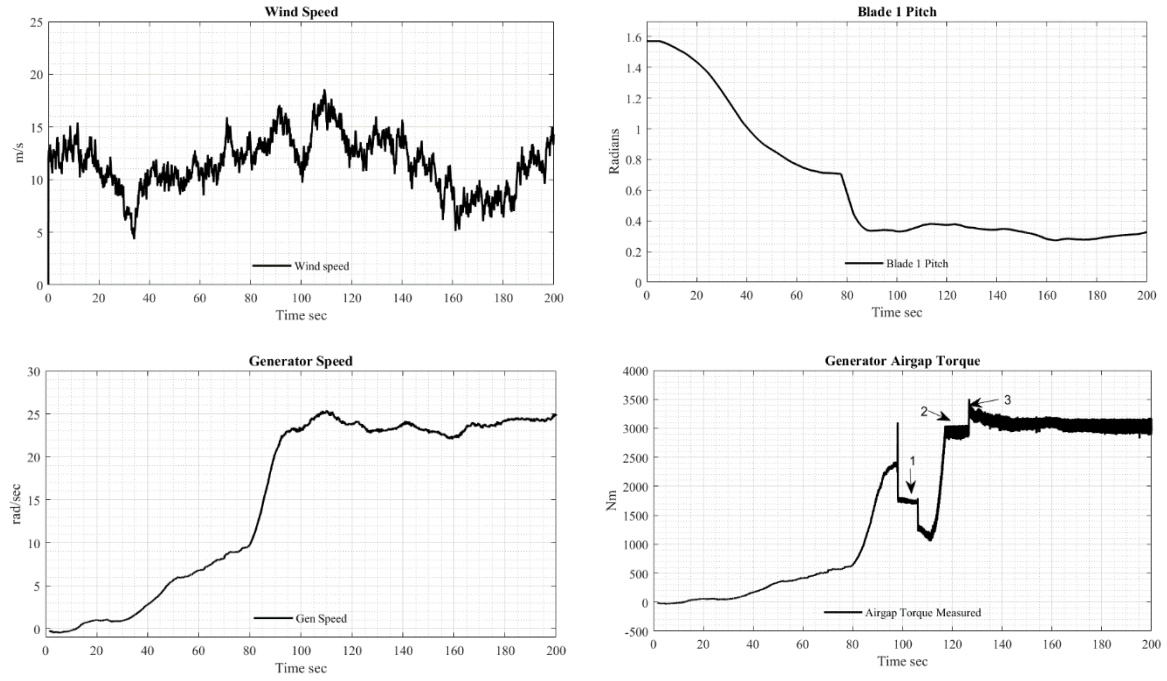

Figure 5-9: Wind speed (top left), Blade 1 Pitch(top right), Generator Speed (bottom left) and Generator Air-gap Torque (bottom right) of the DLC 1-2 12 m/s test case in CHiL test bench – Hard Energisation

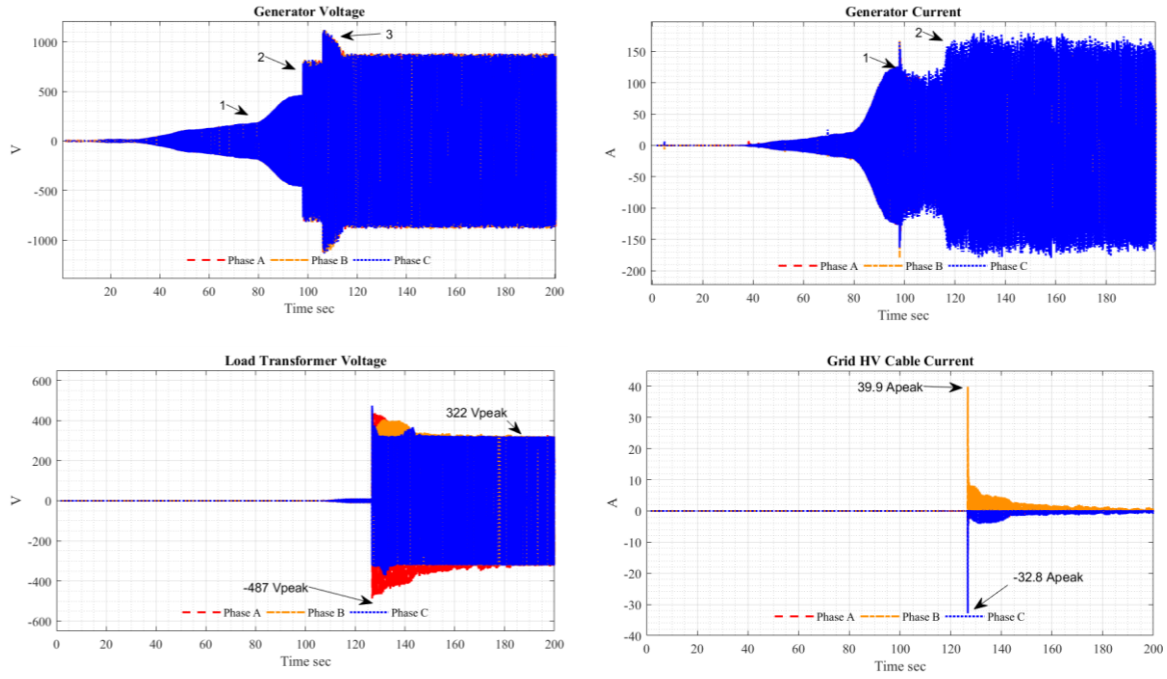

Figure 5-10 Generator voltage (top left), Generator current (top right), Load transformer voltage (bottom left) and Grid side current (bottom right) of the DLC 1-2 12 m/s test case in CHiL test bench – Hard Energisation

In the bottom left figure of Figure 5-10 it is possible to observe the energisation of the Load transformer, which at the beginning shows an unbalanced energisation that later reaches its nominal voltage peak value of 322 $V_{L\text{-}Npeak}$,

This project has received funding from the European Union's Horizon 2020 research and innovation programme under grant agreement No 691714.

which would be equivalent to 227.6 $V_{L\text{-}Nrms}$. The current measurements were taken at the HV cable of the power circuit, since there is no load on the secondary of the load transformer. The HV cables is also subject of the current transient during the hard energisation which peaks up to 39.9 A_{peak} and later is completely reduced down below

5.3.3 PHIL CO-SIMULATION RESULTS

Soft energisation

The soft energisation for the proposed test circuit was successfully validated in different wind conditions and turbulence. All cases were tested with auxiliary loads connected. Here, the test case DLC 1-3 12 m/s is shown. This case uses a nominal wind at 12 m/s with extreme turbulence. This case tests the pitch control carry on the start-up and control the speed regardless extreme wind turbulence. The wind profile used in the test case is shown in the top left of Figure 5-11. In top right of the same figure, it is possible observe the pitch angle throughout the test. It performs a correct start-up of the WT. Firstly pitching in the angle of the blade until it reaches 0.79 rad to accelerate the rotor to 9 rad/s to start power production. Once in power production it manages to maintain the pitch angle in the operation range.

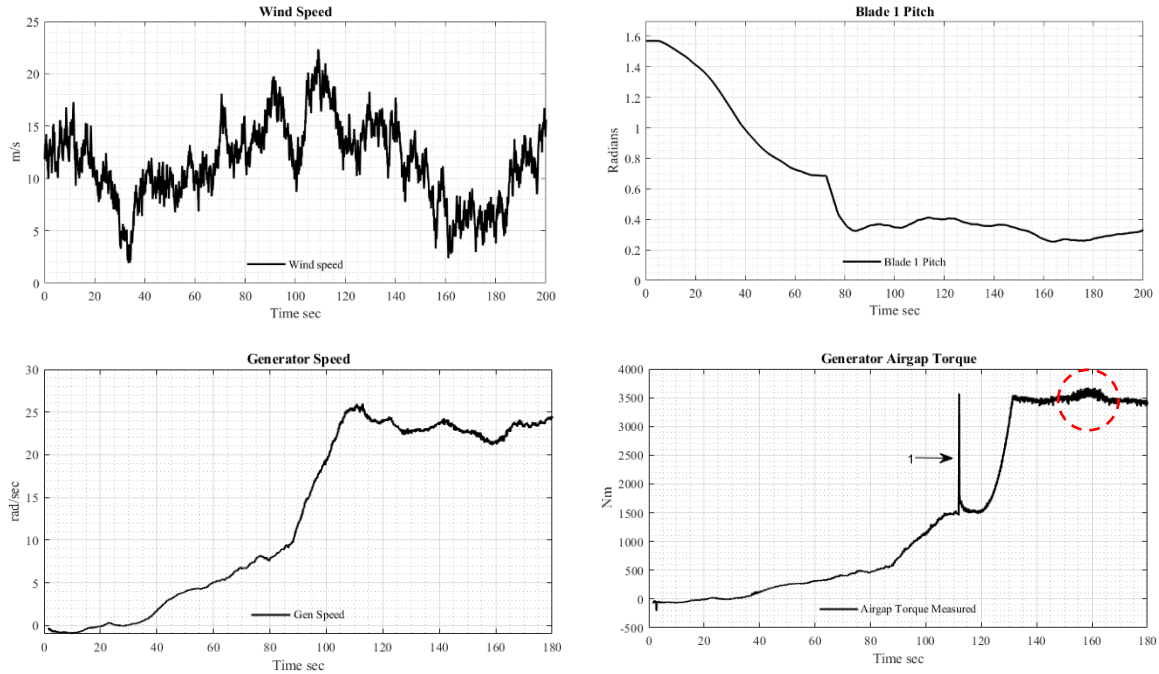

Figure 5-11: Wind speed (top left), Blade 1 Pitch(top right), Generator Speed (bottom left) and Generator Airgap Torque (bottom right) of the DLC 1-3 12 m/s test case in PHiL test bench - Soft Energisation

The generator speed is shown in the bottom left part of Figure 5-11, where the acceleration of the speed increases as the blade pitches in. After ramping up the speed to nominal power production, the effect of wind turbulence is noticeable in the speed variation. The bottom right part of Figure 5-11 shows the generator air-gap torque, the transient seen is from when the converter starts conducting (1). Shortly after the transient the power production

This project has received funding from the European Union's Horizon 2020 research and innovation programme under grant agreement No 691714.

starts increasing the airgap torque. The wind turbulence effect in the air-gap torque can be observed at t = 160 s (circled in red).

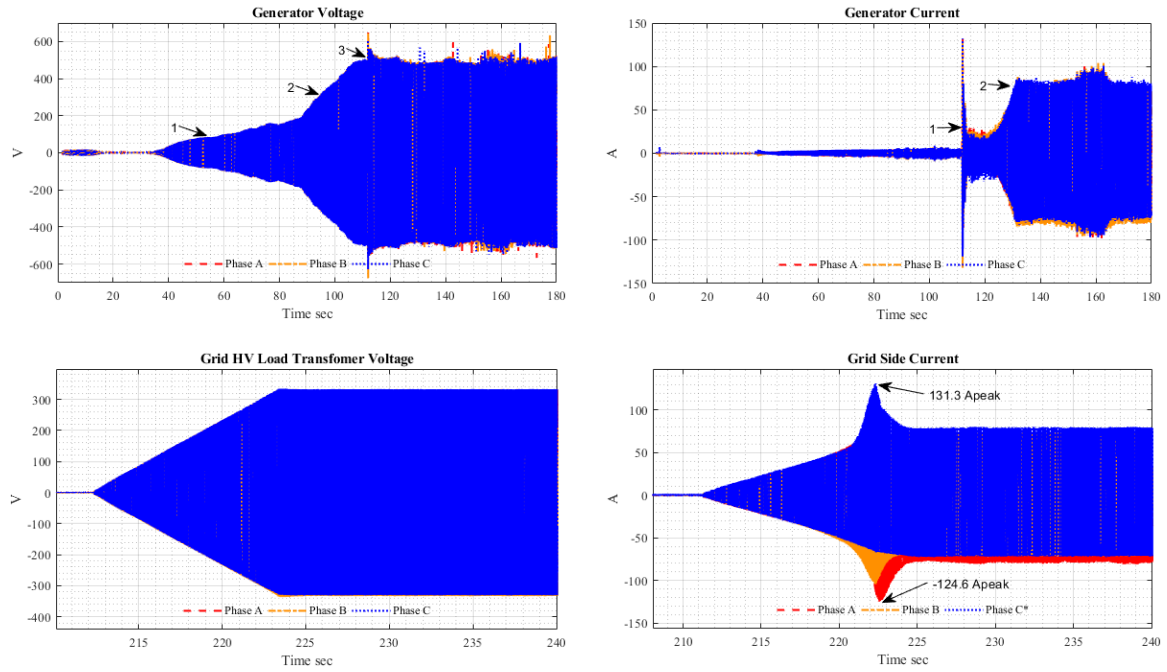

Figure 5-12: Generator voltage (top left), Generator current (top right), Load transformer voltage (bottom left) and Grid side current (bottom right) of the DLC 1-3 12 m/s test case in PHiL test bench –Soft Energisation

The generator voltage as shown in top left part of Figure 5-12 depicts three events throughout the test, first the acceleration of the generator rotor increases the voltage and frequency (1), then is ready to ramp-up to power production increasing to nominal voltage (2). Finally, the converter generator side starts conducting (3). The generator current as shown in top right part of Figure 5-12 sees a current transient caused by the converter conduction, and later a ramp up to power production.

The voltage on the secondary of the load transformer (3) is steadily built to its nominal value without any effects of the wind turbulence. The magnetizing current in the HV Cable is too small and not accurate. However, Figure 5-12 intends to confirm the small energisation current seen in this part of the test circuit and the small peak observed during the energisation.

On the grid side of the converter the soft start of the power circuit is confirmed (bottom left in Figure 5-12) since it is capable to ramp up the voltage in a controlled manner. The voltage reaches the nominal voltage of 235 V_{LNrms} of the secondary winding of the load transformer after 11 seconds. The bottom right part of Figure 5-12 shows the inrush current of the transformers as seen by the converter. The current peaks at 131 A, and later normalizes to a steady state of 55 A.

Hard energisation

The hard energisation is the most demanding test case for the converter controllers due to the high transient currents that could push the wind turbine converter to instability.

This project has received funding from the European Union's Horizon 2020 research and innovation programme under grant agreement No 691714.

For this test there were many attempts to prove it successful and consistent. There were a few successful energisations but most of the attempts failed. This inconsistency in the success was caused by the inrush current seen at the grid side which varies at every attempt due to the remnant flux in the load transformer to be energised. In the failed attempts we observed a higher current that pushes the converter to instability because the power amplifier that emulates the generator reaches its current limit losing its control on the voltage. With these observations, we can indicate that the proposed test bench has a hard limitation to validate the hard start with the given power setup. We are of the opinion that such limitation can be mitigated by a power amplifier with higher power rating, and the instability we observed will not appear in real system. However, this has to been confirmed by another PHiL test bench equipped with power amplifier of higher rating.

Here, test case of hard start PHiL with wind profile DLC 1-2: 12 m/s is presented. This test cases uses nominal wind speed of 12 m/s with normal turbulence, the wind profile throughout the test is shown in top left part of Figure 5-13. The objective of this test case is to prove a successful hard start energisation supported by the GF-FRT functionality. The power circuit for this test case was slightly modified, removing the load bank to allow a higher current transient on the grid side of the converter at the moment of connection of the second part of the power circuit. This was done in order to reach the triggering level of the GF-FRT operation which is enabled when the converter sees a current above 1800 A_{peak}.

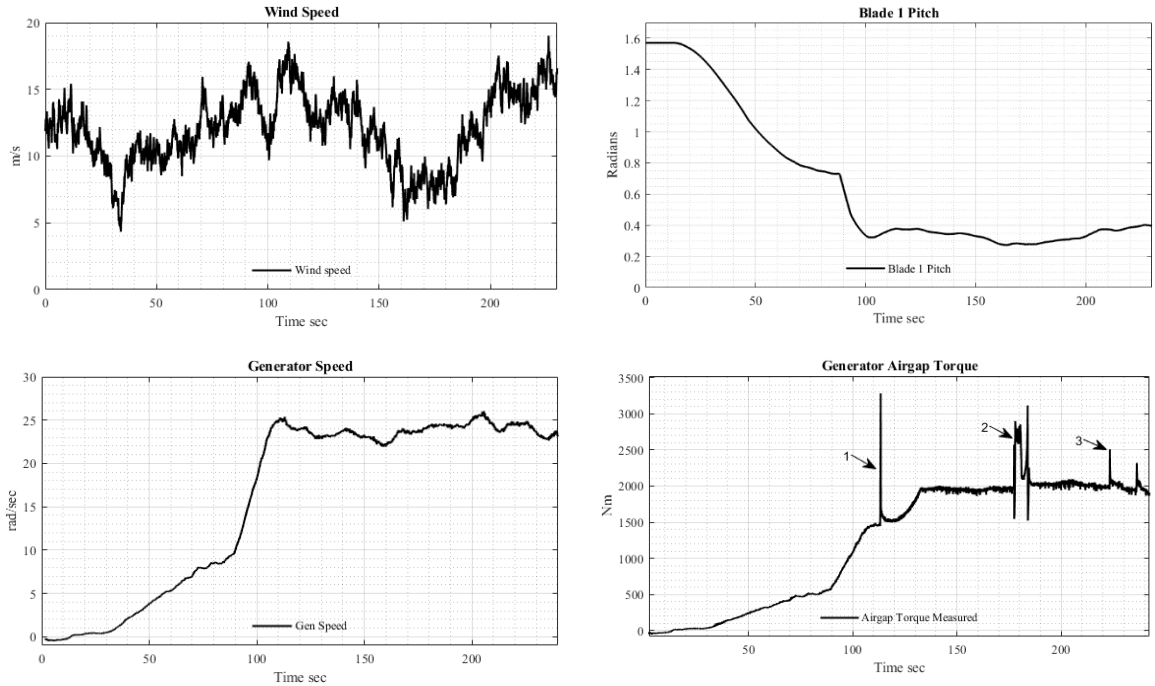

Figure 5-13: Wind speed (top left), Blade 1 Pitch(top right), Generator Speed (bottom left) and Generator Air-gap Torque (bottom right) of the DLC 1-2 12 m/s test case in PHiL test bench - Hard Energisation

The pitch of the wind turbine (top right of Figure 5-13) performs a normal start up sequence. The hard energisation event does not have any effect on the pitch control. The small variations seen in the angle are mainly a response to the turbulence of the wind profile.

This project has received funding from the European Union's Horizon 2020 research and innovation programme under grant agreement No 691714.

The generator speed is shown in the bottom left part of Figure 5-13, it reaches nominal speed around 24 m/s at t = 110 s. The variations seen after t = 110 s are caused by the wind turbulence. During the events of hard energisation, the generator speed is not affected.

The generator air-gap torque (in the bottom right part of Figure 5-13) portrays clearly all the events of the test. First (1) the converter starts switching and ramps up the power production. The first hard energisation occurs at t = 179 s (2), once stable the HV side of the circuit is disconnected with no big transient. Finally, (3) a second hard energisation occurs at t = 222 s.

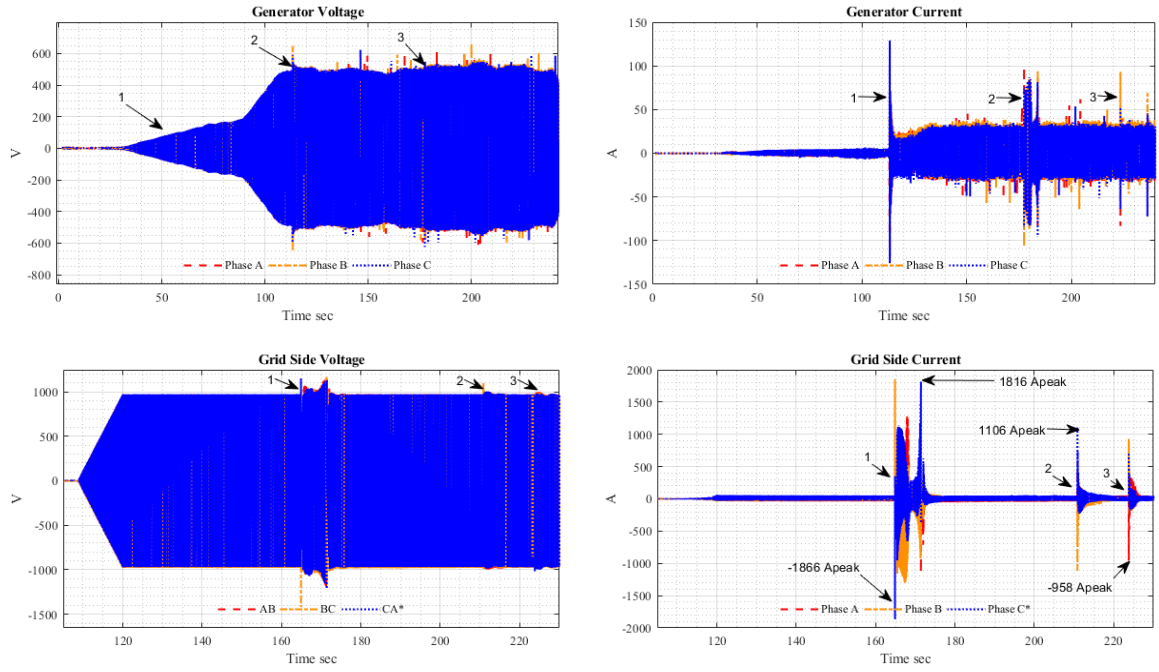

Figure 5-14: Generator voltage (top left), Generator current (top right), Grid side voltage (bottom left) and Grid side current (bottom right) of the DLC 1-2 12 m/s test case in PHiL test bench –Hard Energisation

The generator voltage in top left Figure 5-14 shows the normal ramp up of voltage (1) during start-up, the switching in of the converter (2) and indicates when the hard energisation occurs (3). The later does not really have a significant effect on the voltage. The voltage oscillations seen on the crest of the waveform are mainly caused by the wind turbulence.

The top right part of Figure 5-14 indicates the current behaviour in the generator, where is also possible to observe the hard energisation events on the grid side. First, the converter starts conducting (1). Second, the hard energisation takes place at 179 s (2). The second hard energisation is indicated by (3).

On the grid side the voltage trend (bottom left Figure 5-14), the converter first builds a voltage on the grid side terminals energising the 1 MVA transformer. Once the voltage reaches its steady state the HV side of the power circuit is switched in (1), (2 and 3) are two other hard energisations to test the GF-FRT control algorithm multiple times.

The current of the grid side (bottom right Figure 5-14) portrays the transient current of the hard energisation events. The first hard energisation (1), second hard energisation (2) and third energisation (3). It is important to

This project has received funding from the European Union's Horizon 2020 research and innovation programme under grant agreement No 691714.

mention that the GF-FRT functionality is triggered when the current exceeds the 1800 A limit. Therefore, the second and third hard energisation does not trigger the functionality.

The voltage during the first hard energisation (Figure 5-15) depicts GF-FRT which blocks the conduction of the converter for a short period and builds the voltage. When the GF-FRT was triggered for a second time due to the transformer saturation the voltage was once again blocked (2) and ramped up once more.

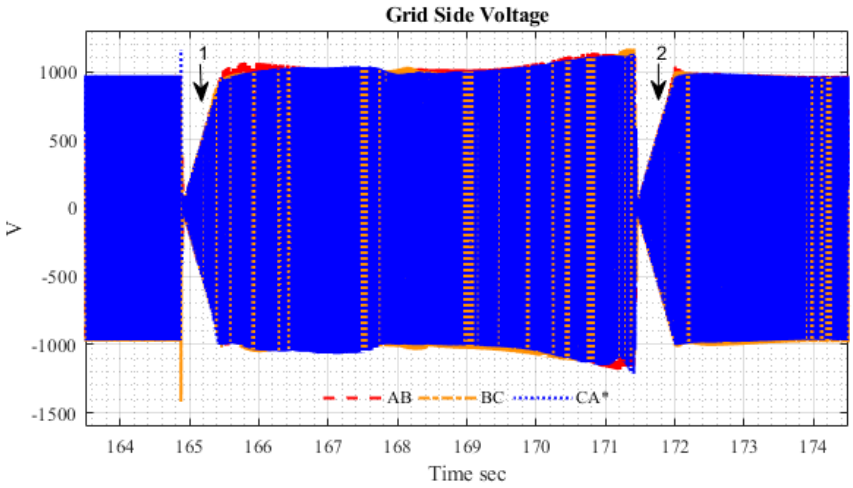

Figure 5-15: HS DLC 1-2: 12 m/s - Grid side voltage GF-FRT capability

A closer look to the current on the first hard energisation is shown in Figure 5-16. In this figure it is possible to observe the functionality of the GF-FRT. The first current transient occurs at 164.9 seconds reaching -1866 A_{peak} which triggers the GF-FRT, immediately the current is blocked, shortly after (200 ms) the current starts to ramp up (1). After 5 seconds it is possible to see the transformer entering saturation, which causes the current in phase C reaching 1816 A_{peak}; the GF-FRT algorithm is triggered once again (2) and prevents further saturation of the transformer.

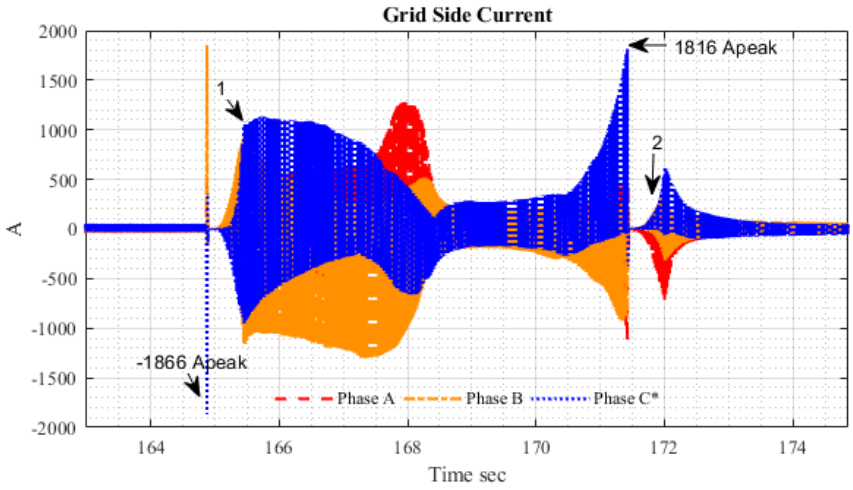

Figure 5-16: HS DLC 1-2: 12 m/s - Grid side current GF-FRT capability

This project has received funding from the European Union's Horizon 2020 research and innovation programme under grant agreement No 691714.

Finally, the voltage on the load transformer confirms the successful hard energisation of the second part of the power circuit (Figure 5-17). In the figure is possible to observe the multiple switching in operations previously explained.

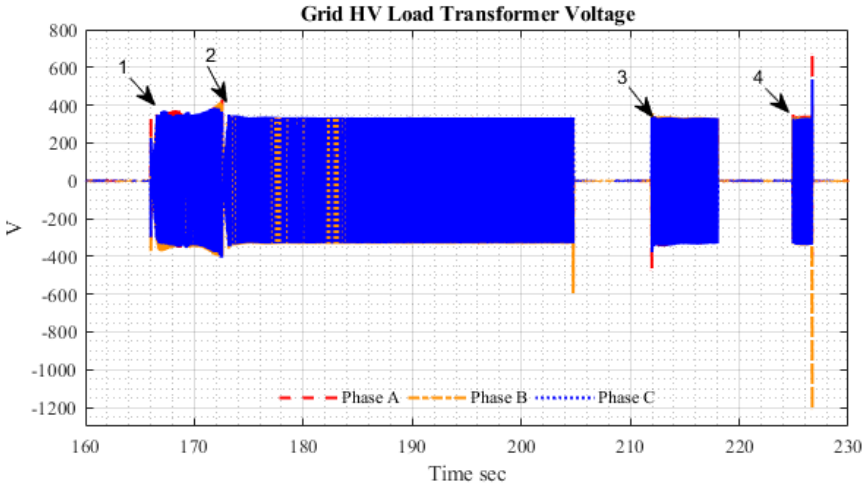

Figure 5-17: HS DLC 1-2: 12 m/s - Grid HV Load transformer voltage trend

5.4 CONCLUSION

The following conclusions can be drawn based on previous sections:

1. **Soft Start:** The soft energisation for the proposed test circuit was successfully validated in different wind conditions and turbulence profiles. It has been possible to confirm that soft start reduces significantly the current and voltage transients seen by the electrical equipment.
2. **Hard Start:** The proposed variant of the grid-forming fault-ride-through function to carry on hard energisation manoeuvres has been proven to be successful in managing the transient currents seen at the moment of switching the circuit and even prevent the transformer from running into saturation mode. This function was tested with the co-simulation base test case DLC1-2 12 m/s i.e. normal turbulence with nominal wind speed. However, the effectiveness and consistency of the proposed variant should be further studied and confirmed by a test bench with a larger power amplifier.
3. **Test Benches:** This research is being adopted on the development of new test benches that take a step forward on the use of HiL and co-simulation for development and validation of advanced WT functions where a holistic assessment is required. This work enables new tools for OEMs that are flexible and cost efficient that could help in the future for certification purposes

This project has received funding from the European Union's Horizon 2020 research and innovation programme under grant agreement No 691714.

6 SUMMARY AND FUTURE WORK

The focus of WP16 of the PROMOTioN project is to investigate potentially crucial interactions between different converter controls and converter technologies on the one hand and the interaction between meshed HVDC offshore grids and offshore collector networks on the other hand. A special emphasis is given on medium- to high-frequency interactions, also called harmonic resonances, within such networks. This deliverable focuses on the system and component behaviour in offshore collector networks.

It is shown that the MMC controls developed in WP2 and the grid forming control of the MMCs developed in WP3 can be applied to real (lab-scaled) hardware and enable the operation of a MTDC network used to export wind power. The results show a very close match between the simulated full-scale model, the simulated lab-scale model and the PHiL test bench if the parasitic resistances that are present in the PHIL test bench are scaled up and simulated for the full-scale model. If these parasitic resistances are not considered, then a difference in the transient behaviour, i.e. especially when regarding the DC voltage in case of a set-point change between the full-scale model on one side and the lab-scale model and the PHIL test bench on the other side can be observed. Investigations on how to reduce these parasitic resistances of the cable connections will be carried out, such that these parasitic resistances are minimized and the transient behaviour of the PHIL test bench and the full-scale model is as close as possible. While the focus of the deliverable regarding the investigations and demonstration of the interoperability of MTDC networks and WPPs are on the steady-state behaviour, the investigations will be extended to dynamic and transient situations, including faults in the offshore collector networks and the MTDC system in deliverable D16.4.

To assess the stability of converter-dominated networks, like offshore collector networks, it is essential to have accurate frequency-dependent impedance models of the network's converters. Within this deliverable, methods are presented and analysed, which can be applied to power hardware components as well as their simulation replica models. The method is applicable for measuring the frequency response of MMCs and WTGs with various control systems when an analytical derivation of the converter impedance is not feasible. Nevertheless, further studies need to be carried out to investigate the effect of the transformer impedance, in particular at high frequencies in the kHz range. Based on the obtained frequency-dependent impedance models, the stability in different offshore collector grid configurations will be analysed in the frequency domain in the up-coming work. To validate the applicability of derived method for the stability analysis, the results will be validated against time-domain simulations and PHiL tests, cf. Figure 6-1.

This project has received funding from the European Union's Horizon 2020 research and innovation programme under grant agreement No 691714.

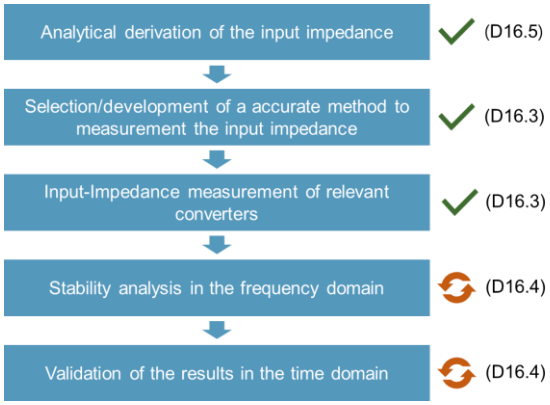

Figure 6-1: WP16 approach regarding the stabiltiy analysis of converter-dominated networks

In addition, the black-start capability of a commercial WT converter is demonstrated using a 1-MW WT converter and its control replica. Therefore, a PHiL and CHiL test setup is established, which can be used in the future for network compliance tests of different power converters.

Nevertheless, the conducted tests have been focused on a single commercial WT converter. As a next step, the joined black-start capability of multiple WT converters in grid forming control will be analysed. This cannot be realised with power hardware or the cubicles of a commercial WT converter. Hence, the investigations are carried out in a CHiL laboratory comprising independent control units to ensure that all converter controls are independent from each other. Again, these results will be document in the final deliverable D16.4 of WP16.

This project has received funding from the European Union's Horizon 2020 research and innovation programme under grant agreement No 691714.

7 REFERENCES

[1] PROMOTioN WP16, “Deliverable D16.5: Implementation of an analytical method for analysis of harmonic resonance phenomena,” Brussels, BE, 2019.

[2] PROMOTioN WP 16, “D16.5: Implementation of an Analytical Method for Analysis of Harmonic Resonance Phenomena,” 2019.

[3] A. Rygg, M. Molinas, C. Zhang and X. Cai, “A Modified Sequence-Domain Impedance Definition and Its Equivalence to the dq-Domain Impedance Definition for the Stability Analysis of AC Power Electronic Systems,” *IEEE Journal of Emerging and Selected Topics in Power Electronics, vol. 4, no. 4,* pp. 1383-1396, December 2016.

[4] A. Rygg, M. Molinas, C. Zhang and X. Cai, “On the Equivalence and Impact on Stability of Impedance Modeling of Power Electronic Converters in Different Domains,” *IEEE Journal of Emerging and Selected Topics in Power Electronics, vol. 5, no. 4,* December 2017.

[5] PROMOTioN WP2, “Deliverable 2.1: Grid topology and model specification,” 2017.

[6] BESTPATHS Project, “http://www.bestpaths-project.eu/en/publications,” 2017. [Online].

[7] Best Paths, “Detailed specification of the demonstrator,” 2016.

[8] PROMOTioN WP16, “D16.7: Updated documentation of the lab set-up, technical specifications and configuration possibilities,” 2019.

[9] Mathworks, “https://www.mathworks.com,” 2019. [Online].

[10] OPAL-RT Technologies, “Technical Description - MMC-based multi-terminal DC transmission system - RWTH Aachen University,” Canada, 2018.

[11] W. Ren, M. Steurer and T. Baldwin, “Improve the Stability and the Accuracy of Power Hardware-in-the-Loop Simulation by Selecting Appropriate Interface Algorithms,” in *2007 IEEE/IAS Industrial & Commercial Power Systems Technical Conference*, Edmonton, Alta., Canada, 2007.

[12] B4.57, Cigre Working Group, TB 604 Guide for the Development of Models for HVDC Converters in a HVDC Grid, Cigre, 2014.

[13] N. W. Miller, J. J. Sanchez-Gasca, W. W. Price and R. W. Delmerico, “Dynamic Modeling of GE 1.5 and 3.6 MW Wind Turbine Generators for Stability Simulations,” 2003.

[14] J. Sun and H. Liu, “Sequence Impedance Modeling of Modular Multilevel Converters,” *IEEE Journal of Emerging and Selected Topics in Power Electronics, vol. 5, no. 4,* pp. 1427-1443, December 2017.

[15] H. Wu and X. Wang, “Dynamic Impact of Zero-Sequence Circulating Current on Modular Multilevel Converters: Complex-Valued AC Impedance Modeling and Analysis,” *IEEE Journal of Emerging and Selected Topics in Power Electronics,* 2019.

[16] J. Lyu, X. Zhang, X. Cai and M. Molinas, “Harmonic State-Space Based Small-Signal Impedance Modeling of a Modular Multilevel Converter With Consideration of Internal Harmonic Dynamics,” *IEEE Transactions on Power Electronics,* pp. 2134-2148, März 2019.

[17] L. Bessegato, L. Harnefors, L. Ilves and N. S., “A Method for the Calculation of the AC-Side Admittance of a Modular Multilevel Converter,” *IEEE Transactions on Power Electronics,* pp. 4161-4172, Mai 2019.

[18] M. Quester, F. Loku, V. Yellisetti and R. Puffer, “Online Impedance Measurement of a Modular Multilevel Converter,” in *IEEE PES Innovative Smart Grid Technologies Europe (ISGT-Europe)*, Bucharest, Romania, 2019.

[19] Y. A. Familiant, J. Huang, K. A. Corzine and M. Belkhayat, “New Techniques for Measuring Impedance Characteristics of Three-Phase AC Power Systems,” *IEEE Transactions on Power Electronics,* pp. 1802-1810, Juli 2009.

[20] H. P. Hall, “How electronics changed impedance measurements,” *Proceedings of the 21st IEEE Instrumentation and Measurement Technology Conference (IEEE Cat. No.04CH37510),* pp. 2-8, 2004.

[21] J. Huang, K. A. Corzine and M. Belkhayat, “Small-Signal Impedance Measurement of Power-Electronics-Based AC Power Systems Using Line-to-Line Current Injection,” *IEEE Transactions on Power Electronics, vol. 24, no. 2,* pp. 445-455,, February 2009.

[22] M. Cespedes and J. Sun, “Adaptive Control of Grid-Connected Inverters Based on Online Grid Impedance Measurements,” *IEEE Transactions on Sustainable Energy, vol. 5, no. 2,* 516-523 April 2014.

This project has received funding from the European Union’s Horizon 2020 research and innovation programme under grant agreement No 691714.

[23] R. Luhtala, T. Roinila and T. Messo, “Implementation of Real-Time Impedance-Based Stability Assessment of Grid-Connected Systems Using MIMO-Identification Techniques,” *IEEE Transactions on Industry Applications, vol. 54, no. 5,* pp. 5054-5063, Sept.-Oct 2018.

[24] T. Roinila, T. Messo and E. Santi, “MIMO-Identification Techniques for Rapid Impedance-Based Stability Assessment of Three-Phase Systems in DQ Domain,” *IEEE Transactions on Power Electronics, vol. 33, no. 5,* pp. 4015-4022, May 2018.

[25] T. Roinila, M. Vilkko and J. Sun, “Online Grid Impedance Measurement Using Discrete-Interval Binary Sequence Injection,” *IEEE Journal of Emerging and Selected Topics in Power Electronics,* pp. 985-993, December 2014.

[26] A. Rygg and M. Molinas, “Real-time stability analysis of power electronic systems,” *IEEE 17th Workshop on Control and Modeling for Power Electronics, COMPEL 2016 : Proceedings,* 2016.

[27] PROMOTioN WP 16, “Deliverable 16.1: Definition and Specification of Test Cases,” 2019.

[28] DNV GL Energy, “Reducing the risks of network restoration. DNV GL’s soft energisation approach.,” 2016.

This project has received funding from the European Union’s Horizon 2020 research and innovation programme under grant agreement No 691714.